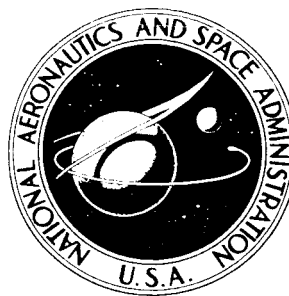


**NASA TECHNICAL
MEMORANDUM**



NASA TM X-1279

NASA TM X-1279

1. TITLE
2. AUTHOR
3. PERFORMING ORGANIZATION
4. REPORT NUMBER
5. DISTRIBUTION STATEMENT
6. PRICE

44-38489
58
1
Thx - 1279 31

**AEROBEE 150 STRUCTURAL AND
AERODYNAMIC PITCH COUPLING**

by J. R. Busse and G. E. Kraft

Goddard Space Flight Center

Greenbelt, Md.

AEROBEE 150
STRUCTURAL AND AERODYNAMIC PITCH COUPLING

By J. R. Busse and G. E. Kraft

Goddard Space Flight Center
Greenbelt, Md.

NATIONAL AERONAUTICS AND SPACE ADMINISTRATION

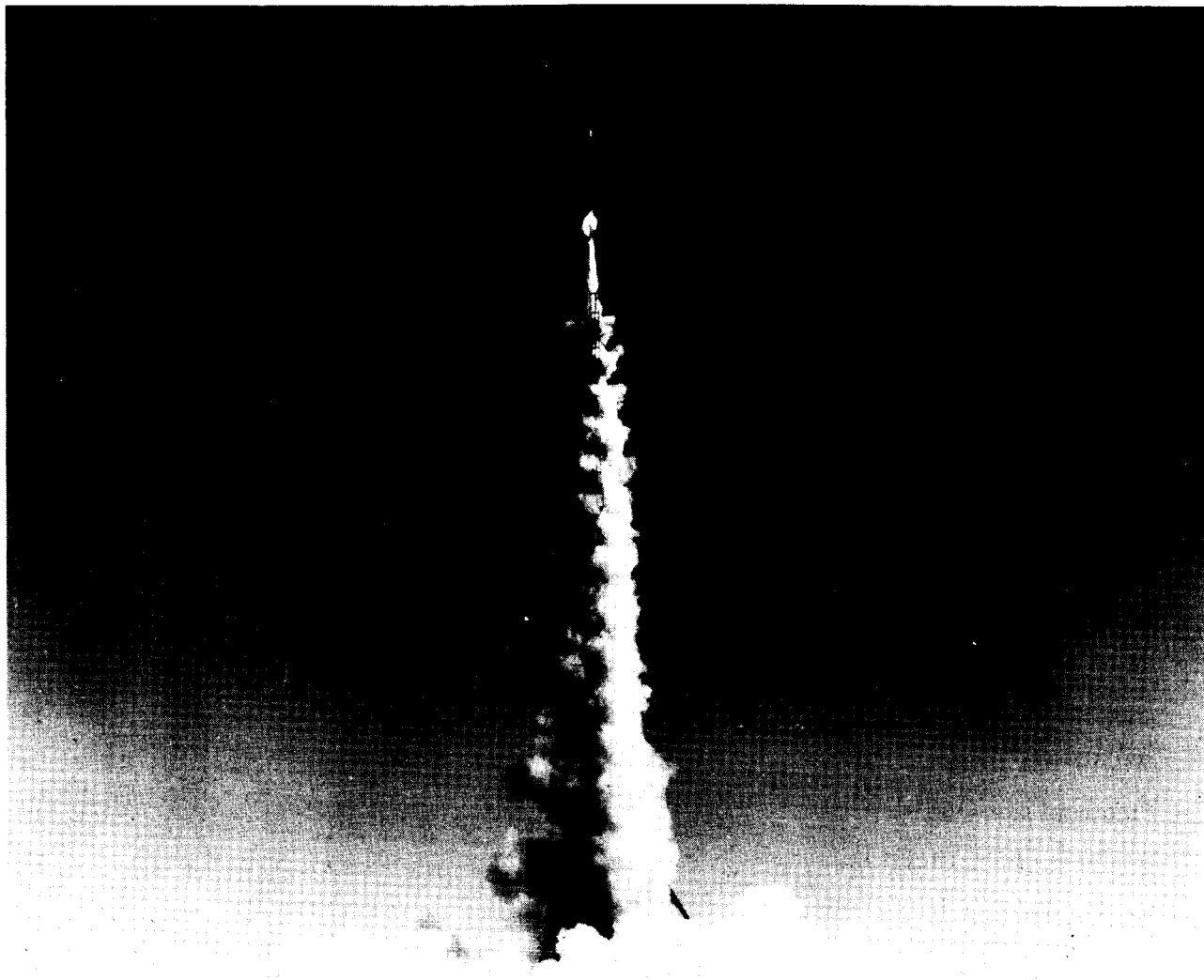
For sale by the Clearinghouse for Federal Scientific and Technical Information
Springfield, Virginia 22151 - Price \$2.50

ABSTRACT

An investigation was undertaken to discover the causes for the failure of NASA Aerobee 150 flights 4.81 GG and 4.86 NA. After analyzing the flight performance data and comparing them with the data for two similar successful flights, NASA flights 4.15 GG and 4.88 GT, it was concluded that the most probable cause for rocket malfunction in each case was a bimodal instability arising from the coupling of an abnormally low body bending mode with the vehicle aerodynamic pitching mode which, in turn, caused yaw (pitch)-roll coupling and lock-in. Corrective measures proposed as a result of this investigation have been instituted, and no similar Aerobee rocket failures have been experienced since.

CONTENTS

Abstract	ii
INTRODUCTION	1
FLIGHT HISTORY	1
Flight Failures of NASA 4.81 GG and NASA 4.86 NA Rockets	3
Comparison of NASA Flights 4.15 GG and 4.88 GT	8
DATA REDUCTION	12
Chamber Pressure	12
Fuel Pressure	12
Oxidizer Pressure	12
Acceleration	12
Velocity	13
Altitude	13
Velocity Vectors	13
Yaw Frequency	14
Pitch Frequency	14
Roll Rate	14
Wind Data	14
Stability Data	14
Analysis of Significant Data	17
CONCLUSIONS	18
ACKNOWLEDGMENTS	19
References	19
Appendix A—Data Plots, Flights 4.15 GG, 4.81 GG, 4.86 NA, and 4.88 GT	21
Appendix B—Flight Data Analysis	41
Appendix C—Definition of Terms	49



Lift-Off Photo, Aerobee 150 WSMR

AEROBEE 150

STRUCTURAL AND AERODYNAMIC PITCH COUPLING

by
J. R. Busse and G. E. Kraft
Goddard Space Flight Center

INTRODUCTION

An investigation was undertaken to determine the causes of failure on NASA Aerobee 150 flights 4.81 GG and 4.86 NA so that corrective action could be taken to avoid similar failure in the future. These two flights were analyzed and the analyses compared with those of the flight results of two similar but successful flights, NASA 4.15 GG and 4.88 GT. The most probable cause of failure of flights 4.81 GG and 4.86 NA appears to have been the result of the dynamic coupling between structural and aerodynamic yaw (pitch) modes which subsequently caused yaw (pitch)-roll coupling and lock-in.

Detailed data plots are provided in Appendix A to support the conclusions arising from this report. This appendix contains many charts which were produced during the reduction of data for successful flights 4.15 GG and 4.86 NA as well as those for flights 4.81 GG and 4.86 NA. Their arrangement provides a rapid means of comparison in each category of data discussed.

Calculations are included in Appendix B to substantiate failure theories arising from the failure investigations.

It is important to note that Appendix C contains definitions for the terminology used in this analysis, since these terms have not been rigorously defined in words by the technical community. Their definition is essential to this analysis and discussion of results.

More information on these rockets and related subjects is given in References 1 through 5.

FLIGHT HISTORY

The evaluations here represent an analysis of the successive malfunctions of two NASA Aerobee 150 Sounding Rockets at the White Sands Missile Range, New Mexico. The two failed vehicles were NASA 4.81 GG, launched on 9 April 1964, and NASA 4.86 NA, launched on 14 April 1964. These vehicles were unprecedented because each used a 20° cone/cylinder nose cone rather than the more common 31-caliber ogive nose and because the payload extension length and

the resultant number of payload joints used exceeded those on other cone/cylinder configurations previously launched.

Although NASA flights 4.81 GG and NASA 4.86 NA exhibited what initially appeared to be solely "roll lock-in" problems, two similarly configured vehicles, NASA 4.15 GG and NASA 4.88 GT, had previously been launched successfully. A joint effort was undertaken by the Space General Corp. (SGC) and Goddard Space Flight Center (GSFC) to investigate the abnormal performance of NASA

Table 1

Flight Statistics.

Flight Statistic	4.15 GG	4.81 GG	4.86 NA	4.88 GT
Sustainer serial no.	NASA 109-3	NASA 102-3	NASA 103-3	NASA 101-3
Booster serial no.	858186	858197	A-117	858180
Sustainer thrust chamber misalignment (in.)*	0.035 at 237°	0.117 at 250°	0.105 at 165°	0.093 at 255°
Total dry weight (lb)	529.9	540.9	548.7	562.4
Net payload (lb)	258.4	271.5	277.2	290.9
Overall length (in.)	321.8	335.0	332.0	330.0
Equivalent extension length (in.)	43.2	56.2	53.4	51.5
Average fin cant (min)**	17.5	17.5	17.5	17.5
Expected burnout roll rate for fin setting and net payload (rps)	1.78	1.76	1.75	1.7
Actual max. roll rate (rps)	1.65	1.1	1.0	1.5
Burnout time (sec)	53.2	52.6	52.6	52.3
Burnout altitude (ft)	130,675	110,246	91,247	120,162
Burnout velocity (fps)	5900	3490	1080	5310
Max. velocity (fps)	5900	3490	3450	5459
Time of max. velocity (sec)	53.2	52.0	41	53.5
Max. acceleration boost (g)	9.9	12.2	9.4	10.0
Max. acceleration (sustainer thrusting) (g)	6.7	6.1	7.3	6.7
Time of max. sustainer acceleration (sec)	51.0	52.0	52.0	52.3
Peak altitude (ft)	626,359	243,084	102,188	652,963
Peak time (sec)	231.3	141.8	77.4	252.6
Number of joints in payload	11	11	11	9
Nose cone type	Cone/cylinder	Cone/cylinder	Cone/cylinder	Ogive

*SGC reading at assembly of sustainer, looking forward with fin I at 0°.

**Fins were set at the maximum cant obtainable on all vehicles.

flights 4.81 GG and 4.86 NA. The performance data from the two similar flights were used as a basis for comparison.

General observations on the data for each flight are made; obvious similarities and dissimilarities are discussed later in detail with explanatory comments to support the derived theories. Table 1 summarizes some of the statistics for each flight.

Flight Failures of NASA 4.81 GG and NASA 4.86 NA Rockets

NASA flight 4.81 GG took place on 9 April 1964. The early motion of the Aerobee rocket remained steady and appeared normal; no abnormal transient responses were observed to result from the tower exit, booster burnout, booster separation, or wind effects. At approximately $T + 29$ seconds, the rocket began to display an abnormal divergent coning motion. The amplitudes observed were small initially, and the frequency was essentially equal to the roll rate. The abnormal rocket coning motion continued and increased in magnitude until approximately $T + 39$ seconds. The coning half angle had grown to approximately 8° by $T + 39$ seconds and the basic frequency had dropped to approximately one-half of the theoretical pitch frequency. This indicated that the classical yaw (pitch)-roll lock-in did not occur up to this time, although the yaw (pitch)-roll coupling had been initiated.

Pitch and yaw plots for this flight are shown in Figures 1 and 2 compared with plots for flights 4.15 GG and 4.88 GT. The abnormal pitch and yaw motions are clearly evident after $T + 29$ seconds; prior to this time 4.81 GG appears better behaved than either 4.15 GG or 4.88 GT, since it exhibits less pitch and yaw motion.

At an altitude of approximately 66,550 feet ($T + 39.5$ seconds), a premature ejection of the nose tip occurred while the vehicle was still burning. This occurrence was preceded by a secondary oscillation (read on gyro outputs) of approximately 3.5 cps. Following the nose tip ejection, yaw (pitch)-roll coupling began, accompanied by excessive aerodynamic drag. The roll rate began to decrease rapidly from 1 rps to the pitch frequency and by $T + 42$ seconds the rocket was fully "locked-in." During the time from $T + 40$ to $T + 42$ seconds, the observed pitch-yaw frequency rose slightly and equaled the roll rate, which was diminishing. At $T + 40$ seconds the coning half angle was greater than 15° , and at $T + 42$ seconds it had reached a stable value of 35° .

Figure 3a shows the center of motion shifts observed on flight 4.81 GG. The vehicle achieved an apogee of only 42.5 statute miles (at $T + 141.8$ seconds), and since the altitude control system (ACS) had no opportunity to start pointing at programmed targets (because of the low altitude attained), no experimental data were obtained. Two cameras and two spectrographs contained in the payload sections were to have obtained spectral data of certain stellar and nebular sources. The parachute deployed successfully, and the payload was recovered in excellent condition.

Flight 4.86 NA took place on 14 April 1964. The rocket performance during the initial seconds of flight appeared to be normal, just as for flight 4.81 GG. At approximately $T + 30$ seconds

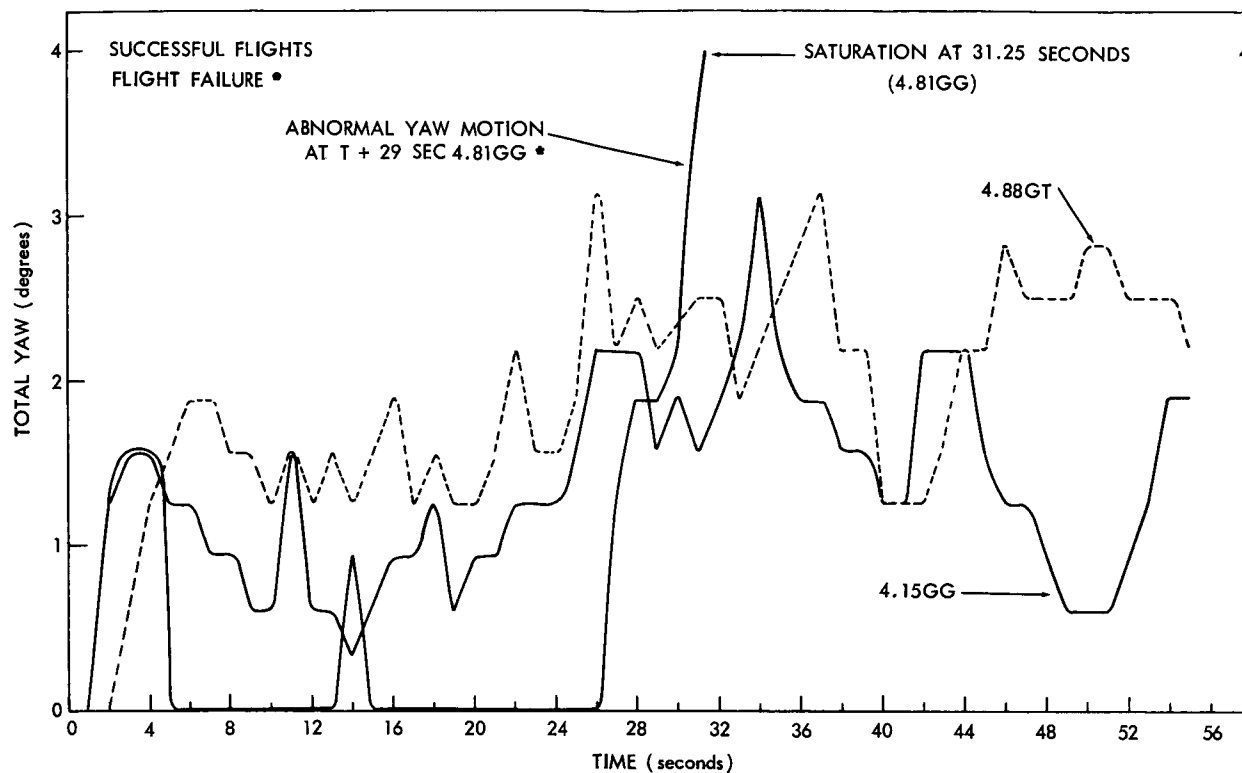


Figure 1—Yaw vs. time; comparison of flights 4.15 GG, 4.81 GG, and 4.88 GT.

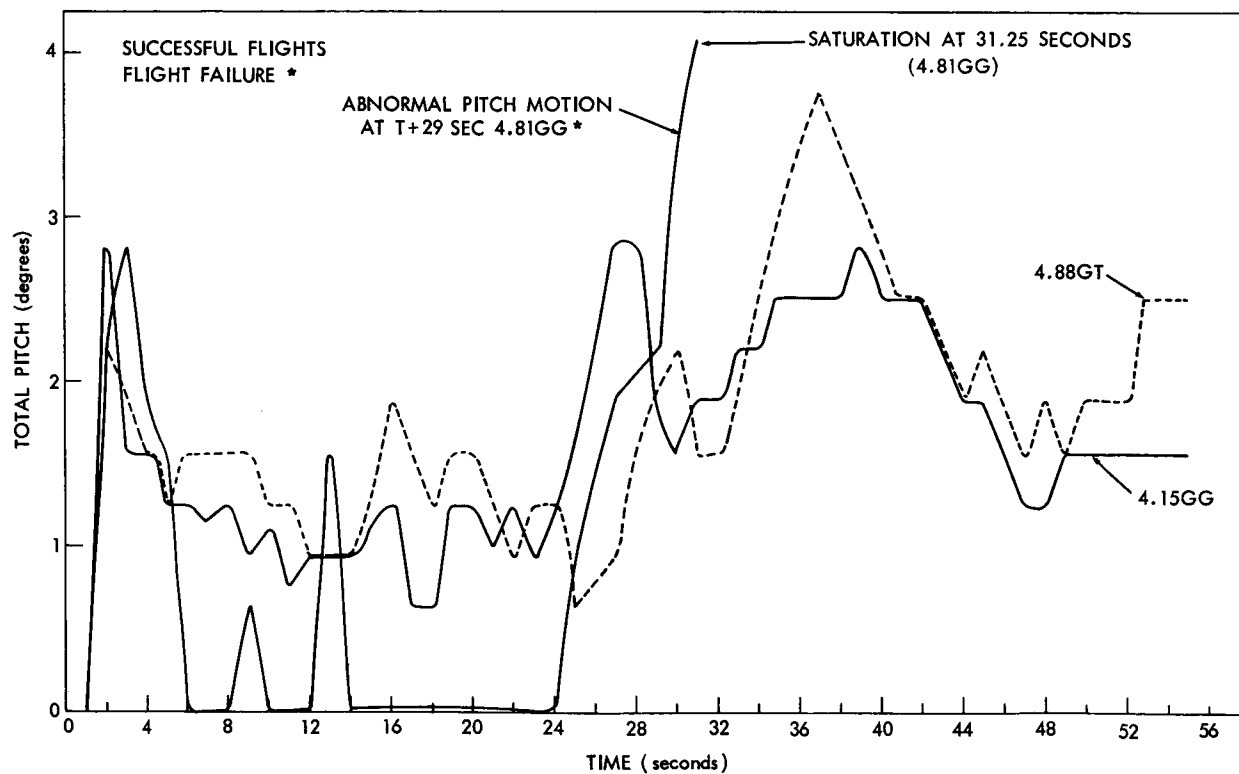


Figure 2—Pitch vs. time; comparison of flights 4.15 GG, 4.81 GG, and 4.88 GT.

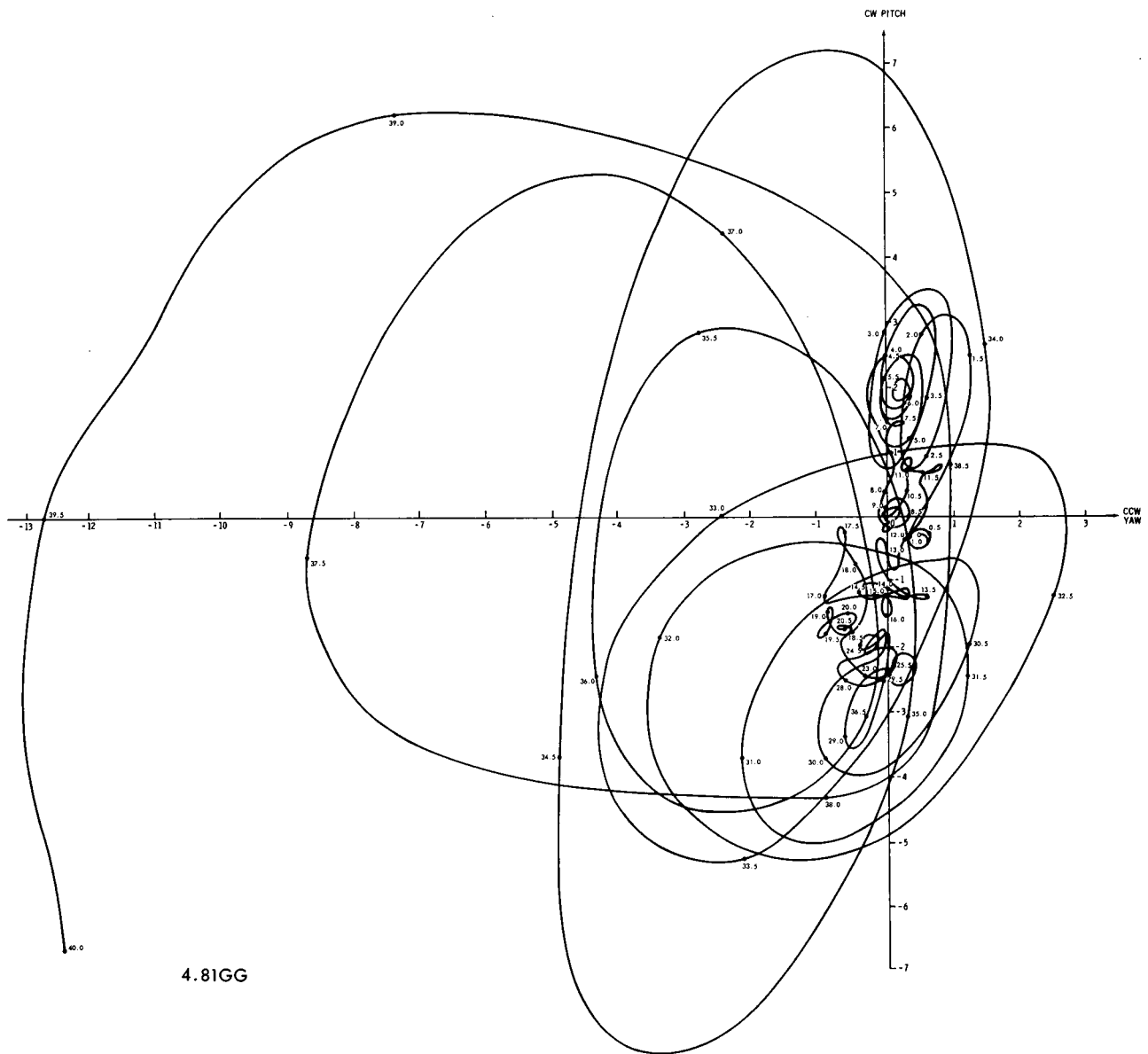
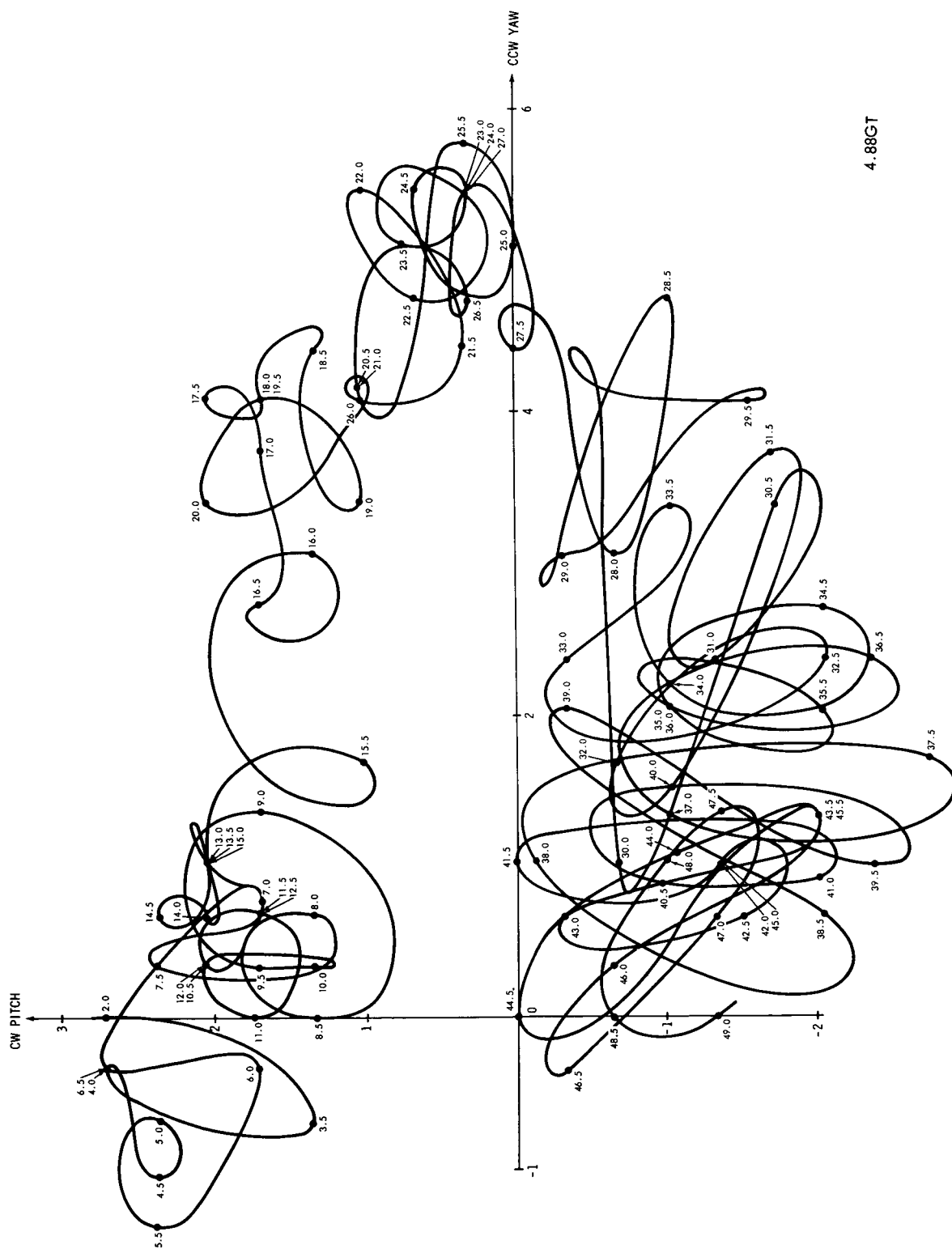


Figure 3a - ACS yaw position vs. ACS pitch position, flight 4.81 GG.
(Coordinates are in degrees; points are in seconds from lift off.)

Figure 3b – ACS yaw position vs. ACS pitch position, flight 4.15 GG. (Coordinates are in degrees; points are in seconds from lift off.)



4.88GT

Figure 3c -- ACS yaw position vs. ACS pitch position, flight 4.88 GT. (Coordinates are in degrees; points are in seconds from lift off.)

the vehicle started coning similarly to the 4.81 GG, and at T + 38 seconds it reached the yaw (pitch)-roll resonance point. Gyro data received indicated a pitch rate of 60° per second at this time.

The angle of attack continued to open up as a result of yaw (pitch)-roll coupling. Figure 4 shows roll rate plotted against time for this flight. At T + 42 seconds the vehicle was locked-in and extremely large and erratic coning angles resulted after this point. The stable coning motion that had been observed on 4.81 GG after lock-in was not in evidence on 4.86 NA: the accelerometer continued to register erratic accelerations until T + 49 seconds and dropped to 0 at T + 50 seconds (Figure 5). It is assumed that the ejection of the nose tip on 4.81 GG probably contributed more regular post lock-in motion than 4.86 NA. Note in Figure 6 that the vertical velocity of 4.86 NA began a sharp decline at approximately 41 seconds and continued to drop steadily.

Although the tip ejected at 61.5 seconds, no experimental objectives could be realized since the ACS failed to function with such erratic vehicle performance. The vehicle attained a peak altitude of only 18.2 statute miles. The parachuted payload was successfully recovered.

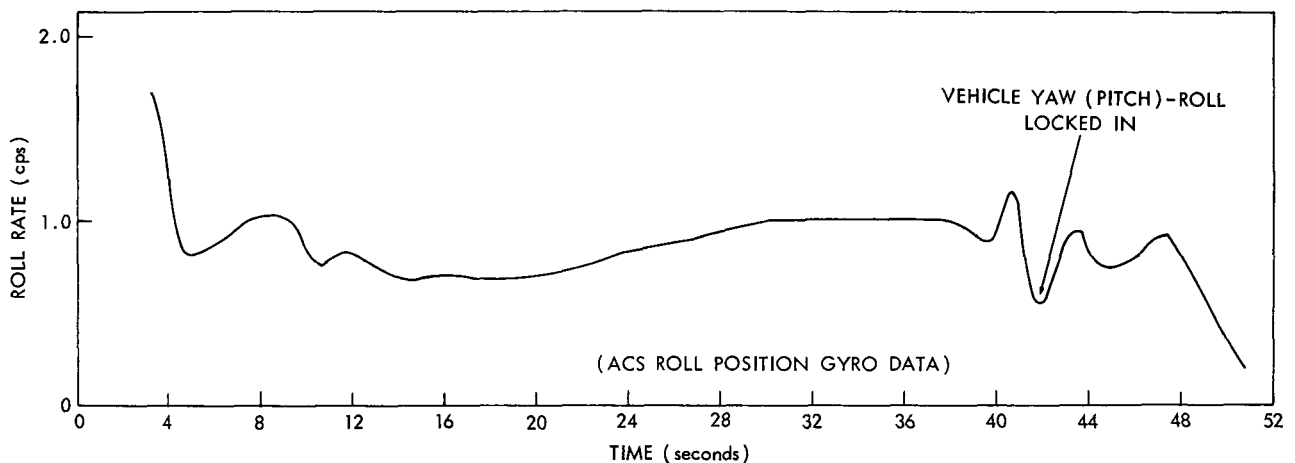


Figure 4—Roll rate vs. time, flight 4.86 NA.

Comparison of NASA Flights 4.15 GG and 4.88 GT

Flight 4.15 GG occurred on 2 April 1964. In terms of rocket performance the vehicle was considered successful, but the experimental objectives were not attained because the ACS failed to align with the gyros to point the rocket at inertially programmed targets.

The launch and flight of 4.15 GG was normal. Some transient responses due to tower exit disturbances, booster burnout, booster separation, and wind were indicated in the first seconds of flight; however, these responses were not considered abnormal.

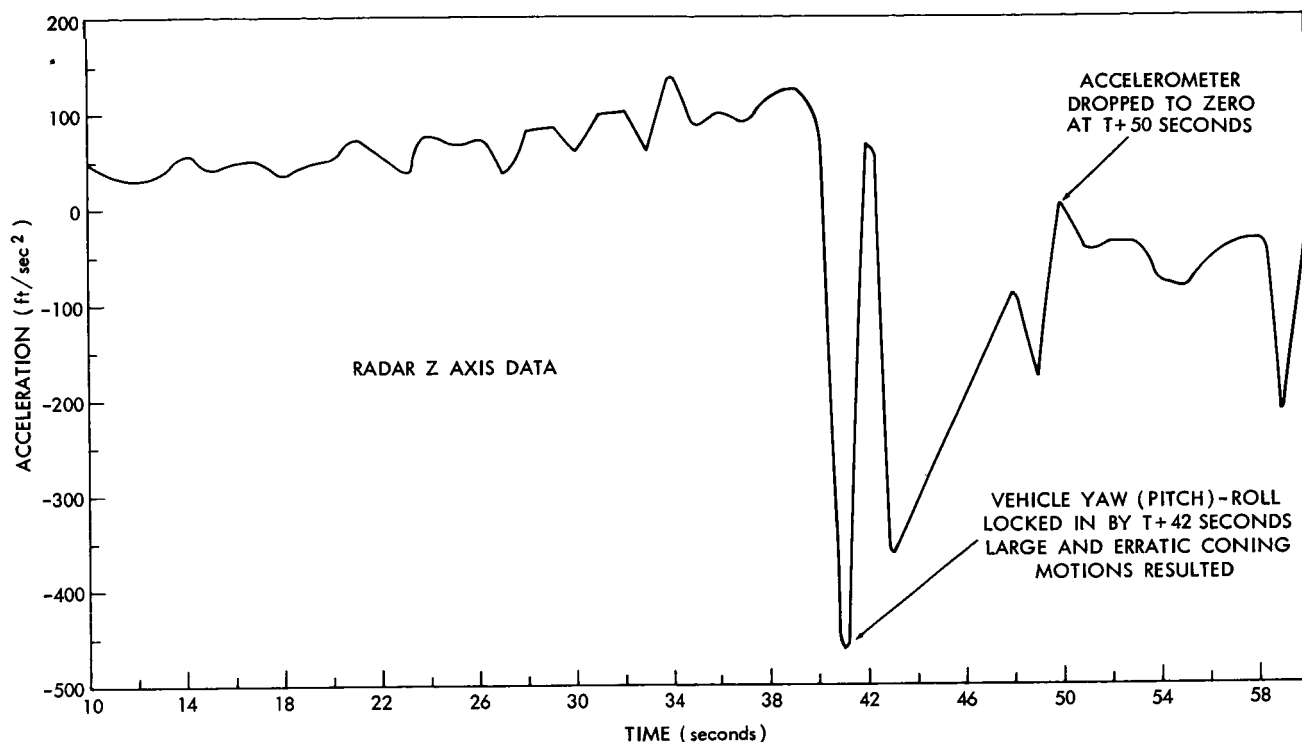


Figure 5—Acceleration vs. time, flight 4.86 NA.

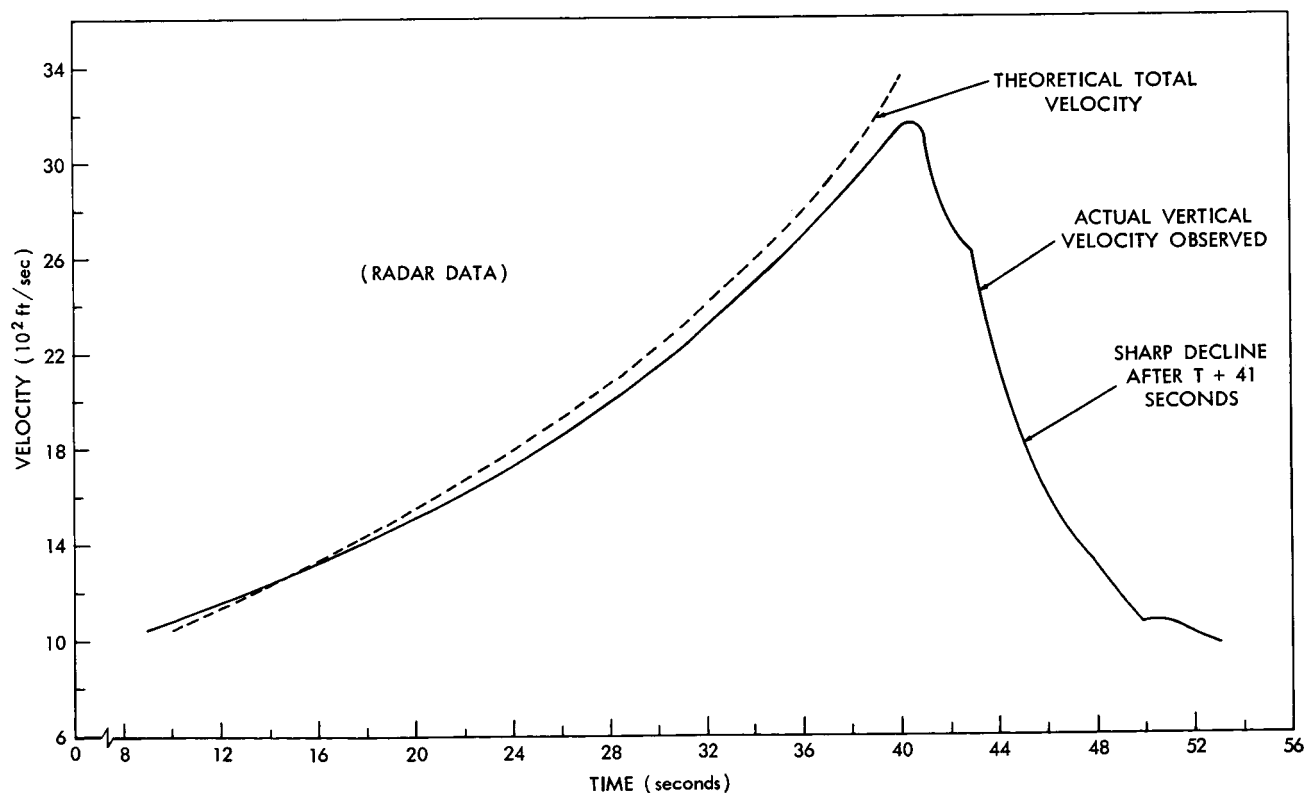


Figure 6—Actual vertical velocity compared with theoretical total velocity in flight 4.86 NA.

Figure 7 is a comparison plot of roll rate and theoretical pitch frequency for the two failed flights and the two successful flights, 4.15 GG and 4.88 GT.* Figure 3b shows the sizeable shifts in the center of motion of rocket 4.15 GG which occurred between $T + 8.5$ and $T + 34$ seconds. These shifts make it difficult to determine the exact nature of the rocket's motion; however, the motion was determined to be a mixture of transient oscillations at the pitch frequency and fairly steady oscillations at the roll rate. The oscillations at the roll rate were attributed primarily to thrust chamber and other structural misalignment.

After about $T + 34$ seconds, the motion of the rocket on the position gyro pitch and yaw traces became more easily discernible. Two distinct frequency components were evident—one slightly below the natural pitch frequency and one equal to the roll rate. Although the oscillation at the pitch frequency closely approximated the theoretical pitch frequency calculated for the flight, some coning-type motion was present. There was no evidence of coupling during yaw (pitch)-roll resonance which occurred between $T + 39$ and $T + 40$ seconds.

The rocket attained a peak altitude of 118 statute miles in 235 seconds as predicted, with tip ejection occurring at $T + 85$ seconds. The parachute package deployed successfully and a recovery was accomplished as planned.

Flight 4.88 GT was successfully carried out on 28 January 1964 at White Sands; the rocket reached a peak altitude of 114 statute miles. The rocket and all instrumentation performed as expected; this indicated good rocket control and stabilization.

Large and frequent pitch and yaw motions by the rocket and sizeable transient frequency responses were indicated prior to $T + 31$ seconds (Figure 3c). As in flight 4.15 GG, the motion became more regular near yaw (pitch)-roll resonance (Figure 7). The position gyro outputs had indicated prior to this time that the frequencies were composed of a mixture of transient pitch responses (the result of tower exit, booster separation, and wind shears) and roll rate frequencies. At yaw (pitch)-roll resonance, large transient disturbances of short duration were observed. These were followed by motions which were primarily at the natural pitch frequency, rather than at the roll rate as observed on flight 4.15 GG. Thrust chamber misalignments not measured during rocket build-up were a possible contributing cause of the rapid trim changes near resonance. No signs of yaw (pitch)-roll coupling or yaw (pitch)-roll lock-in were evident.

The recovery system functioned as planned and the payload was in excellent condition.

The principal points of physical comparison for each flight vehicle are:

1. All vehicles contained long payloads, although the payloads on successful flights 4.15 GG and 4.88 GT were not as long as those on failed flights 4.81 GG and 4.86 NA.
2. Vehicle 4.15 GG had a cone/cylinder nose, a 43.2-inch extension length, a 258.4-pound net payload, and 11 joints.

*The theoretical pitch frequency curves are presented since actual frequencies cannot be determined from available flight data. However, the differences between the 300-lb pitch frequency curve and the actual expected pitch frequency curve would be very small.

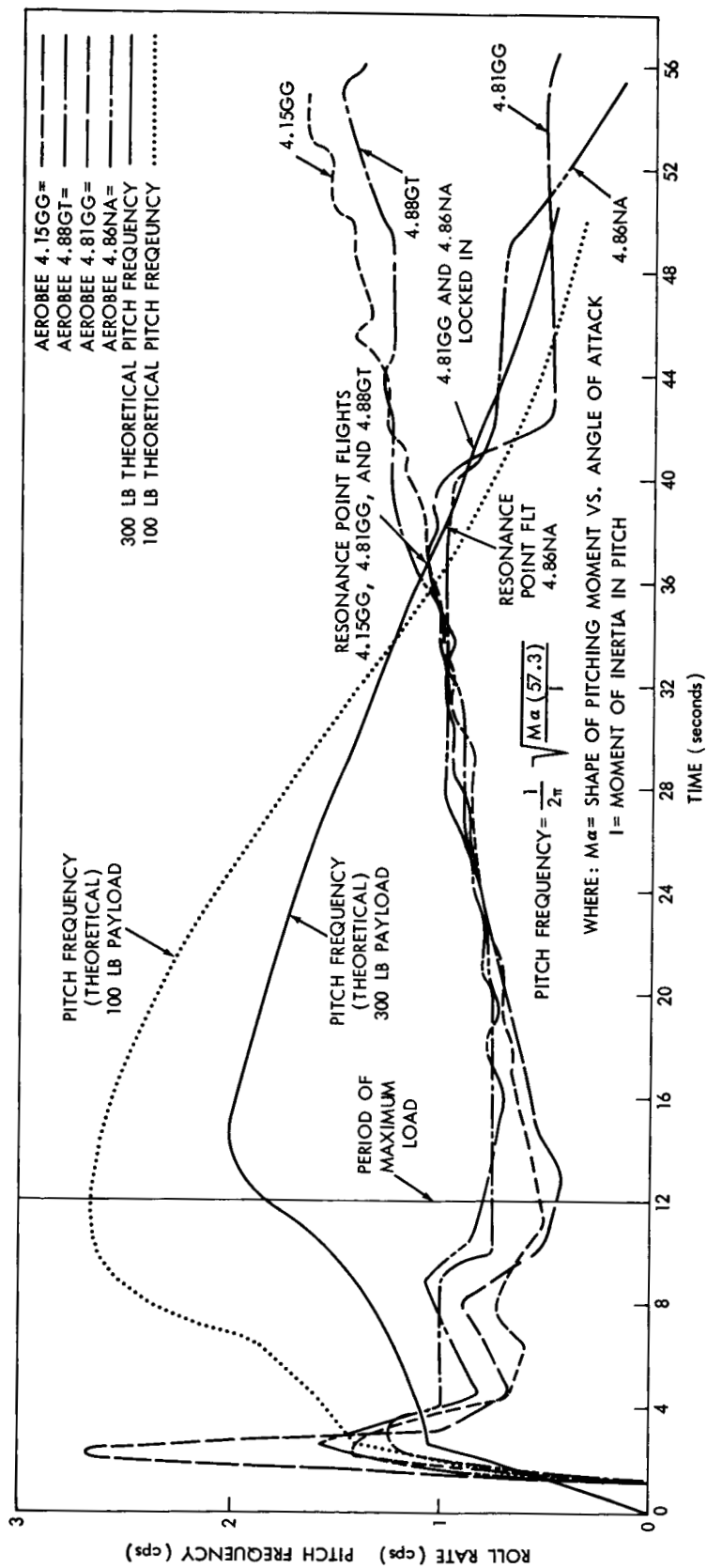


Figure 7—Roll rate and theoretical pitch frequency vs. time; comparison of flights 4.15 GG, 4.81 GG, 4.86 NA, and 4.88 GT. (One-hundred-pound theoretical pitch curve is exhibited to show the relatively small variance in pitch frequency which results from large variations in payload weight.)

3. Vehicle 4.81 GG (failed flight) had a cone/cylinder nose, a 56.2-inch extension length, a 271.5-pound net payload, and 11 joints; its nose was ejected at 39 seconds.
4. Vehicle 4.86 NA (failed flight) had a cone/cylinder nose, a 53.4-inch extension length, a 277.2-pound net payload, and 11 joints.
5. Vehicle 4.88 GT had an ogive nose, a 51.5-inch extension length, and a 290.9-pound net payload, but only 8 joints.

DATA REDUCTION

All available performance and telemetered data for each flight were compiled, reduced, and examined. Wherever possible, these data were combined to facilitate comparative analyses of performance characteristics for each of the flights. The complete data are contained in Appendix A.

Chamber Pressure

The chamber pressure plots of all four vehicles were examined (Figure A1). No patent evidence of thrust chamber contribution to the malfunction of flights 4.81 GG and 4.86 NA was indicated. The plots for each vehicle indicate a steady chamber pressure with no extreme or unusual fluctuations. An initial surge of pressure was noted for each; however, this is a normal start occurrence.

Fuel Pressure

Fuel pressure was not monitored on 4.15 GG. The plot which includes fuel pressure for 4.81 GG (Figure A2) indicates normal pressure levels during the burning phase. The plot for 4.86 NA indicates normal pressure levels during burning, with the expected reduction as the ACS despins the vehicle. The 4.88 GT plot also indicates normal burning pressure levels and pressure reduction after burnout for despinning.

Oxidizer Pressure

Oxidizer pressure was not monitored on 4.15 GG or 4.81 GG. Figure A3 shows oxidizer pressure for flights 4.86 NA and 4.88 GT. No reduction in pressure is observed in the plot for 4.86 NA, which indicates that yaw maneuvers, to be activated by the ACS, did not take place as planned. (This could be expected because of erratic rocket performance.) The reduction in pressure, starting at $T + 89$ seconds on the plot for 4.88 GT, indicates the beginning of the sequence of yaw maneuvers for this vehicle; the continuing decrease is representative of ACS gas usage.

Acceleration

The acceleration plots for each rocket, Figure A4, indicate that all the rockets exhibited normal booster acceleration levels, as well as the normal acceleration dip occurring when each vehicle

passed through the period of maximum load ($T + 12$ to $T + 16$ seconds). Although the plots for 4.15 GG and 4.88 GT indicate some fluctuations in acceleration, they are consistent with normal flight trajectories during the remainder of the flight path.

Vehicle 4.81 GG and 4.86 NA, however, exhibited normal acceleration fluctuations up to, and after, the $T + 40$ to $T + 46$ second period. During the period between $T + 40$ and $T + 46$ seconds, these rockets exhibited some abnormal changes in acceleration and they were especially drastic for Flight 4.86 NA. Since chamber pressure was normal for these flights during the same period, and there were no other obvious anomalies that could have caused such a reaction, it is apparent that erratic vehicle maneuvers are responsible for the fluctuations measured by the accelerometers.

Velocity

Vertical velocity was plotted for each flight and compared with theoretical velocities (Figure A5). The comparison indicates that actual vehicle performance compared favorably with the theoretical velocity in each case for time up to $T + 40$ seconds (the average yaw (pitch)-roll resonance time). There was not an unusual amount of rocket motion in flights 4.81 GG and 4.86 NA to cause a performance loss for the vehicle until that time. After $T + 40$ seconds, however, the effect of the aerodynamic drag and coning that occurred with yaw (pitch)-roll coupling and subsequently with yaw (pitch)-roll lock-in is evident.

Altitude

The altitude plots (Figure A6) reflect the time-velocity relationships for each flight. Curves indicating a theoretical trajectory are also included for flights 4.81 GG and 4.86 NA.

Velocity Vectors

The velocity vector plots shown in Figure A7 for 4.86 NA and 4.88 GT indicate the actual orientation of the vehicle velocity vector in space. The nominal change in orientation is indicative of the response of the vehicle to winds and other transient effects and to the gravity turn. In the case of 4.88 GT, this variation reflects a normal change throughout the burning phase. The magnitude of change in the azimuth of 4.86 NA, which became significant at 34 seconds, is indicative of abnormal vehicle motion. It is noted that the azimuth change became magnified at 40 seconds, which is coincident with the period of abnormal acceleration noted earlier.

It was also observed that the azimuth varied in approximately an east-west direction, starting with approximately a 1 cycle/second frequency and deteriorating to 1/2 cycle/second. When this was compared with the roll history of 4.86 NA, it was noted that this frequency tends to follow the roll frequency. This correlation suggests that during the period discussed the forward end of the vehicle was shifting back and forth in approximately a single plane, following the roll frequency. An imbalance of payload mass could cause this behavior. Such imbalance would be a major contributor to end joint play and resonance coupling.

Yaw Frequency

Comparison of the yaw frequency of NASA vehicles 4.81 GG and 4.86 NA with that of vehicles 4.15 GG and 4.88 GT (Figure A8) shows no apparent relationship of yaw frequency to the problem. Both the magnitude and rate of change in frequency are of a lower order for vehicles 4.81 GG and 4.86 NA. If this criterion were a predictable measure for failure, the reversed relationship might be expected. The observed differences by themselves are therefore insignificant to failure.

Pitch Frequency

Although pitch frequency was not monitored on 4.86 NA, it was obtained for flight 4.81 GG. From a comparison of the pitch frequency plot of flight 4.81 GG with pitch data for flights 4.15 GG and 4.88 GT (Figure A9) it is evident that the successful flights showed higher pitch levels. The rate of change of flight 4.88 GT was also of a higher magnitude than that of the other two flights. As is the case with yaw frequency, however, pitch frequency alone does not necessarily affect the success or failure of the rocket.

Roll Rate

The roll data for all four vehicles (Figure A10) indicated normal levels during the booster phase and normal fluctuation at the time of maximum load (at approximately $T + 12$ seconds). For flights 4.15 GG and 4.88 GT, the roll rate continued to rise through burnout.

The roll rates of 4.81 GG and 4.86 NA are observed to increase in a normal manner, after passing through the period of maximum load until $T + 30$ seconds. At this time, approaching the pitch (yaw)-roll resonance frequency, they both show erratic changes in rate, with a later decrease indicative of pitch (yaw)-roll lock-in.

Wind Data

The atmospheric winds at launch were compared (Figure A11) to deduce if any shears could affect the vehicles structurally. An evaluation of wind velocity and azimuthal shifts obviates the possibility that the vehicles could be so affected. Any such degradation would normally be expected of flight 4.15 GG, and that flight was successful in terms of rocket performance.

Stability Data

Center of Gravity (CG)

The curves of CG against time (Figure A12) are presented only as a comparison between vehicles. These curves do not reflect the actual variation (which is not practically measurable) but they are based on weigh-in values and theoretical propellant usage.

The curves from 0 to 2.5 seconds reflect the presence of the booster, which drag-separates at booster burnout. Thereafter, they reflect propellant usage. No anomalies, such as an improper propellant mixture ratio, are indicated which would have changed the curve.

Center of Pressure (CP)

The CP data (Figure A12) compare the CP location, in calibers from the nose tip, and the time. These data reflect actual flight performance (altitude and velocity vs. time), but the Mach number on which CP is based was derived by using a standard atmosphere. At the time these data were reduced, the actual flight environment was not available. A review of the speed-of-sound data indicates that the Mach number would change by only about 0.06 if the actual atmosphere had been used. This difference would produce a negligible change in the CP location. The CP location is quite consistent up to $T + 40$ seconds in the vehicles under study. They would not be expected to be exactly the same, because the location reflects both vehicle length/diameter (fineness) ratio and Mach number. The variation after $T + 40$ seconds for 4.86 NA and 4.81 GG reflects the decrease in velocity.

Static Margin

The static margin is the difference in calibers between the locations of the CG and the CP of the vehicle, with the CP always being aft of the CG for a stable vehicle. Criteria existing prior to these flights required that the minimum margin be greater than 1.5 calibers. Since none of the vehicles had margins that small (Figure A12) we may conclude that this margin was not a cause of failure. As an additional safety factor, the minimum static margin must now be greater than 2.0 calibers.

Restoring Moment Coefficient C_{M_α}

The moment coefficient C_{M_α} is the product of the static margin SM and the normal force coefficient C_{N_α} which increases as the Mach number M decreases. Thus we see that, conversely, as Mach number decreases (for values of $M > 1$) C_{N_α} increases, and the CP moves aft, causing the margin to increase also. The combination of these forces produced a rise in C_{M_α} in 4.81 GG after $T + 40$ seconds and an increase of the static margin in 4.86 NA (Figure A12). Thus, if the coefficient increases and the velocity remains constant, the restoring force also increases.

Restoring Moment (M_α)

The curves of M_α in Figure A13 indicate that the restoring force of all vehicles was quite similar throughout powered flight. The decreased velocity of the malfunctioning vehicles counteracted the increase in C_{M_α} .

Moment M_α would also be expected to increase with angle of attack if all other parameters remain constant. It can be concluded that the velocity was reduced to such a low magnitude that M_α continued to decrease regardless of the angle of attack or the increase in C_{M_α} .

Speed of Sound

Because performance predictions have been based on the data in Reference 6, the speeds of sound for actual flight atmospheric conditions was compared with those given in that standard in Figure A14. The speed of sound in the atmosphere seen by 4.81 GG and 4.86 NA was lower during their trouble period than that in the standard atmosphere. An evaluation of the slight increase in Mach number seen by the vehicles, and the consequent shift forward of the CP, produced a reduction in margin of the order of 0.05 caliber. Since the margin deduced by using the standard atmosphere never was less than 2.0 calibers, a change of this small magnitude was not enough to cause aerodynamic instability. Thus, this was not significant to the failure.

Atmospheric Density

A number of the calculations of forces acting on the vehicle are based on the atmospheric density, including the restoring force (M_a). The actual flight atmospheres for each of the failed and successful flights were compared with the standard (Figure A15). Since all flight atmospheres observed were equal to, or more dense than, the standard atmosphere up through 100,000 feet, where the vehicles would be most responsive to any variation, the conclusion was reached that, in all cases, the forces acting to restore the vehicles to their normal attitudes were actually somewhat greater than those plotted in the restoring moment curves.

Number of Joints in Payload

The comparison of the number of joints in the payload sections in Figure A16 suggests the first solid clue to the cause of failures. The two failed vehicles are among the longest flown and each contained eleven joints. It is thus suspected that the effect of joints on the structural rigidity leads to failure.

Although flight 4.15 GG also contained eleven joints, its payload section was more than 10 inches shorter than that of either of the failed vehicles. Presumably the structural integrity and dynamic stability were improved by this length decrease and no yaw (pitch)-roll coupling occurred during the period of resonance.

Payload Length and Static Margin

The location of static margin on the failed vehicles of sizeable payload length was also significant in the investigation (Figure A17). It is possible that the static margin should not be a constant value to be established for all Aerobee vehicles, but that the minimum margin between CG and CP should increase as the vehicle length increases. Until more analytic data become available in this area, the minimum accepted static margin at burnout for typical Aerobee rocket configuration has been increased. Thus, the margin of stability (in calibers) has been improved to reduce apprehension that subsequent failure might result due to low static stability.

Analysis of Significant Data

Aerobee 150 vehicles employing long extensions and heavy payloads with many joints and cone/cylinder nose cones have exhibited a propensity toward roll lock-in with accompanying catastrophic yaw (pitch) effects. After comparing flights 4.81 GG and 4.86 NA with two similar successful flights, these failures seem basically due to a bimodal instability arising from the coupling of an abnormally low body bending mode with the vehicle aerodynamic pitch mode. This coupling, further, seems to be caused by excessive end play in the joints of the payload section. Yaw (pitch)-roll lock-in was a logical result of the structural-aerodynamic coupling which preceded it. The static margins, although slightly lower than those shown in theoretical curves, were not considered to be dangerous at the time of flight; however, this experience has led to further considerations which indicate that larger margins might be desirable. The received acceleration histories, motor performance data, and tracking data all had failed to provide any significant evidence of a rocket motor malfunction. The effect of wind shears during these flights is not considered a contributing cause to the failures.

Normally, after launch, the rocket's natural pitching frequency reaches a maximum at 12 seconds and decreases while the roll frequency increases with time. The two frequencies are the same at approximately $T + 40$ seconds of flight time. At this critical time of flight, if some abnormal condition causes the two frequencies to couple at resonance and later lock-in, effects such as those observed on flights 4.81 GG and 4.86 NA can be expected to result. The rocket's roll rate, unable to increase above the rocket's basic yaw (pitch) frequency, drops off drastically with the yaw (pitch) frequency. When this occurs, the angle of attack opens up and very large coning motions are observed. Instability continues with the accompanying effects of increased drag and an abrupt deterioration of velocity performance. Both failures (4.81 GG and 4.86 NA), when compared with two similarly configured successful flights (4.15 GG and 4.88 GT), clearly illustrate these phenomena. Figure 7 clearly shows the abnormal roll behavior of the failed flights compared with the roll behavior of successful similar flights. Note the severe drop in the roll rate for flights 4.81 GG and 4.86 NA and how they couple and later lock-in with the theoretical pitch frequency (300-lb payload curve).

Every attempt was made to compare flight performance data of similar successful and unsuccessful flights to substantiate the validity of the conclusions deducted as a result of this bimodal study. Specific calculations arising from this effort were made prior to the launching of the next Aerobee rocket, flight 4.67 NP, to verify the assumptions made and, to make changes so that another possible failure would be avoided. SGC performed aerolastic computations to substantiate this theory. The method and results of the analysis are provided in Appendix B. Although the analysis is not a rigorous solution to the rocket bimodal instability problem, it does provide a nominal quantity of computations which indicate the probable existence of the bimodal instability phenomenon. Considerably more complex work would have to be performed to prove the form of bimodal instabilities and their amplitudes; however, these computations provide a plausible explanation for the two flight failures and an evaluation of the structural properties required to produce the interaction of payload joint free play and stiffness. These computations, when compared with all analyzed flight data, render a positive deduction that dynamic coupling

between structural and pitch modes can indeed produce instabilities and frequencies of the type observed for flights 4.81 GG and 4.86 NA.

CONCLUSIONS

The primary cause for the malfunctions of the NASA flights 4.81 GG and 4.86 NA was structural and aerodynamic yaw (pitch) coupling. The coupling frequencies were the result of an excessive amount of end play caused by the large number of joints in the longer and heavier payload section of the rocket. To avoid similar failures, the following procedures have been initiated:

1. Sixteen additional screws have been added to increase the rigidity and decrease rotation of payload joints when long payloads with more than 40 inches of payload extensions are used or when two joints are located in close proximity to each other at the aft end of the payload in a rocket configuration. This is by far the most significant change and should prevent similar failures in the future. An improved joint design is being developed by the Sounding Rocket Branch Engineering Section and should be ready for flight in 1966.

2. When possible, the length of the payload is restricted by revised payload design; if long payloads are required, ogive nose cones are recommended, in lieu of cone cylinder noses, to obtain increased stability - a result of the lower nose lift of the ogive which has a fineness ratio of 5-1. The cone-cylinder has a 3-1 fineness ratio.

3. The skin thickness of the tail can has been increased in order that the buckling resistance of the tail section in cases of high booster acceleration may be increased. This is primarily a safety factor, as tail-can loading on the flights in question was not considered great enough to cause structural or thrust misalignment problems which could in turn have produced the observed phenomena.

4. More precise fin alignment checks, and thrust chamber alignment checks have been instituted. The final fin and thrust chamber alignment checks are performed after the rocket tail cylinder has been installed the final time, making the measurements as representative of flight conditions as possible.

5. The interface of fin and tail can has been modified to permit increased fin cant which can produce higher roll rates on rockets with heavy payloads.

6. Bending test and sustainer and payload dynamic balancing operations have been instituted where applicable on payloads with long or unusual configurations. The bending tests identify structural deficiencies in the payload, while dynamic balancing eliminates one destabilizing moment which can potentially cause pitch (yaw)-roll coupling.

7. More thorough instructions for payload assembly, including torquing procedures for rocket screw joints and payload alignment procedures, have been provided for the rocket preparation personnel.

8. Preflight checks and preparations have been revised and up-dated and are strictly monitored by the NASA-GSFC vehicle manager responsible for the flight. The material in Reference 7 is the primary document that was issued to improve the definition of 150 field operations.

9. Limiting criteria for Aerobee 150 flights have been established as follows:

- (a) Static margin > 2 calibers minimum
- (b) Roll rate at burnout > 2 rps < 3 rps
- (c) Thrust chamber misalignment < 0.200 in., and
- (d) Maximum payload length, 147.8 in.

These are general criteria only and, as conditions warrant, the requirements may be raised or lowered depending on the final payload configuration, e.g., length, weight, number of joints, distribution of joints, forebody configuration, and protuberance. No similar NASA Aerobee failures have occurred since these corrective measures were instituted. This covers flights of which many were similar to 4.81 GG and 4.86 NA.

ACKNOWLEDGMENTS

The authors gratefully acknowledge the work of Mr. A. W. Ernest of the Space General Corporation for his assistance in performing detailed aerolastic computations and also the cooperation of Space General personnel in reducing and analyzing the voluminous data involved in this investigation. Thanks are also due to Mr. W. G. Moon, without whose valuable assistance the manuscript could not have been prepared.

(Manuscript received November 19, 1965)

REFERENCES

1. Aerojet-General Corporation, Azusa, California, "Dynamic Analysis, Aerobee Sounding Rocket," Special Report 1467, July 1958.
2. Cronvitch, L.L., and Amsler, B.E., "Pitch-Yaw-Roll Coupling," in: *North Atlantic Treaty Organization, Advisory Group for Aeronautical Research and Development*; AGARD Report 353, 1965.
3. Space General Corporation, "A Study Program on Aerobee 150A Roll-Coupling," p. 4311, July 1963.
4. "Stability and Spin-yaw Resonance in Sounding Rockets," Report on the panel discussion held at the Canadian Aeronautics and Space Inst. Annual General Meeting, Winnipeg, Canada, May 9, 1963.
5. Swanson, R. G., and Rubin, M., "Motion After Burnout of NIKE Cajun Sounding Rocket Ascending Through Atmosphere," Special Report No. 1605, Aerojet General Corp., May 1959.

Appendix A

**Data Plots, Flights 4.15 GG, 4.81 GG,
4.86 NA, and 4.88 GT**

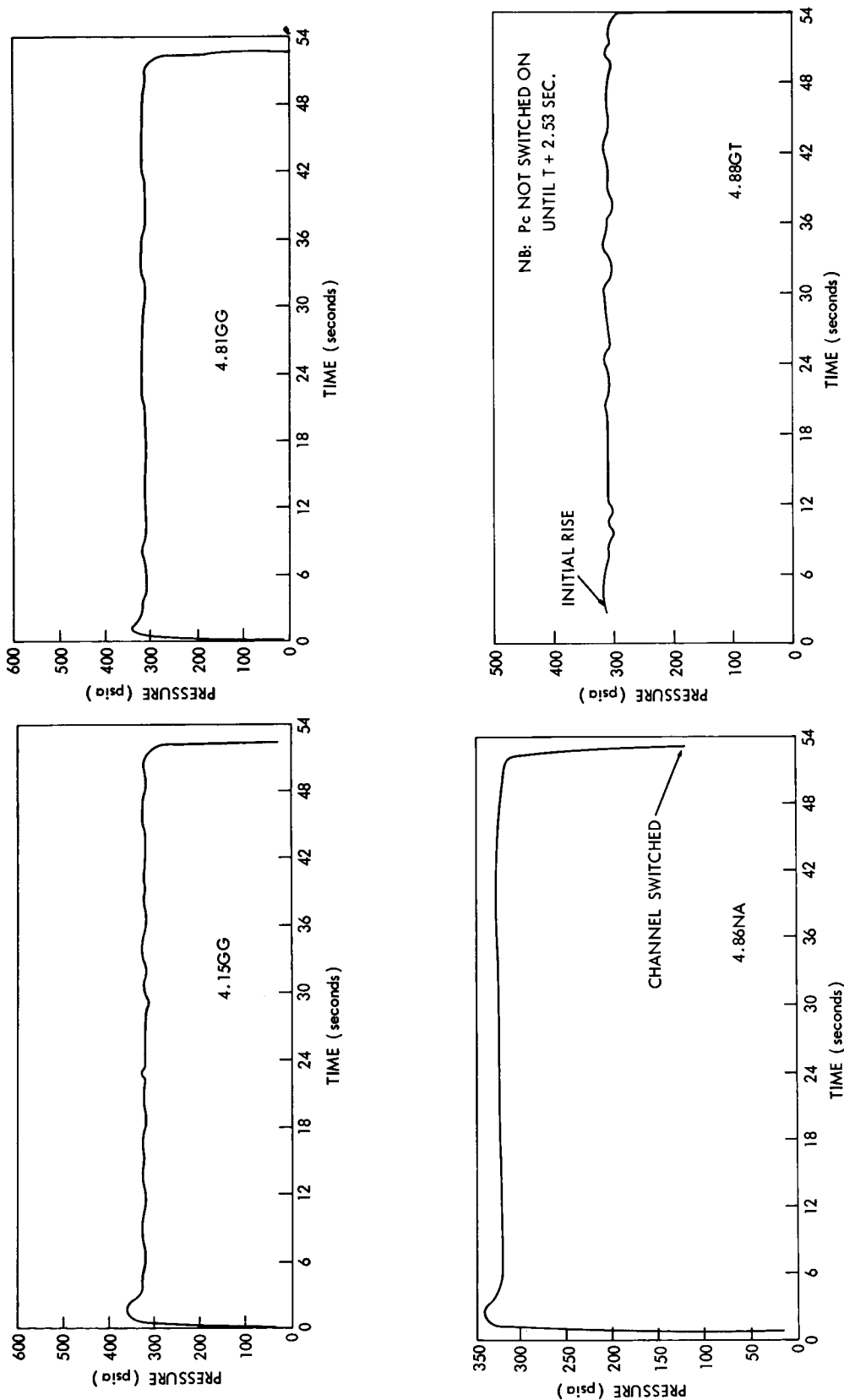


Figure A1—Chamber pressure vs. time; comparison of flights 4.15 GG, 4.81 GG, 4.86 NA, and 4.88 GT.

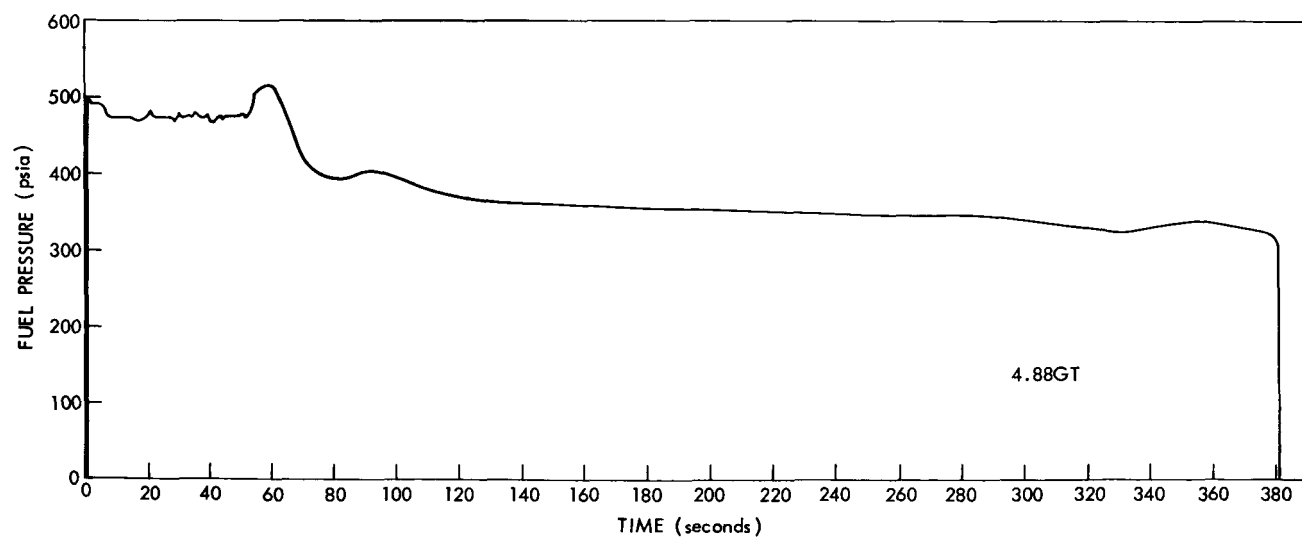
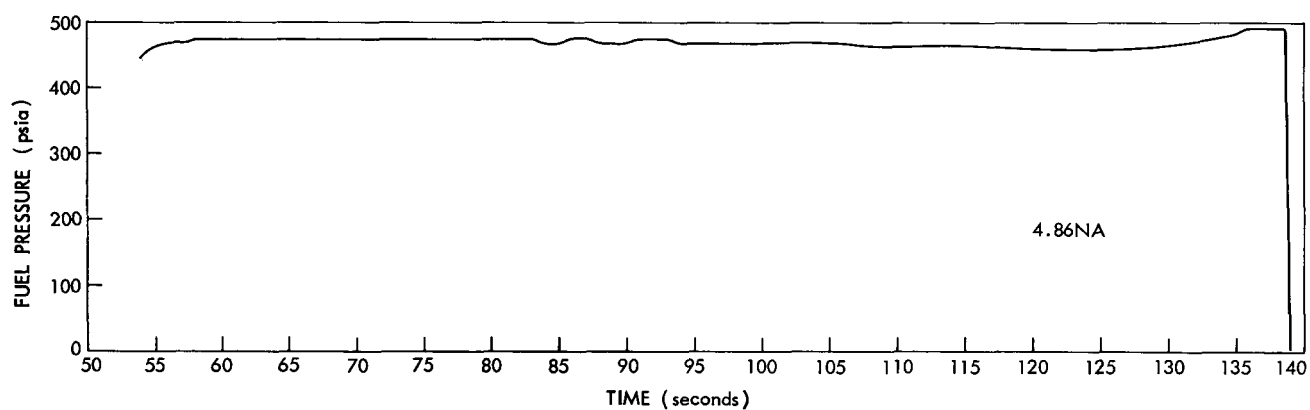
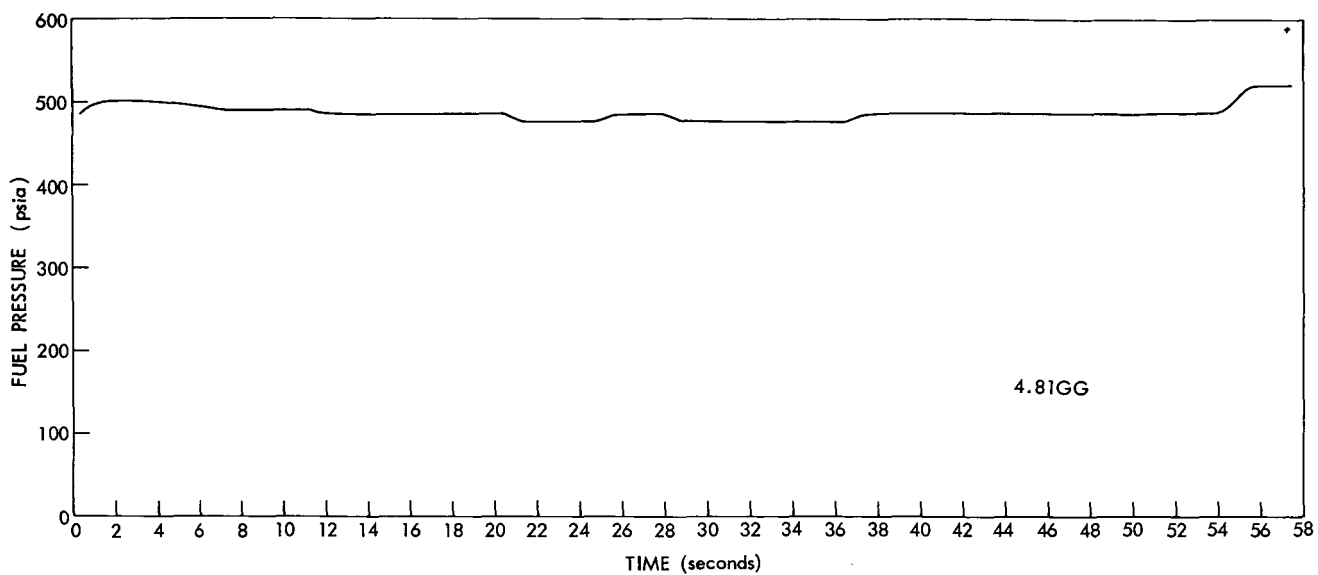


Figure A2—Fuel pressure vs. time; comparison of flights 4.81 GG, 4.86 NA, and 4.88 GT.

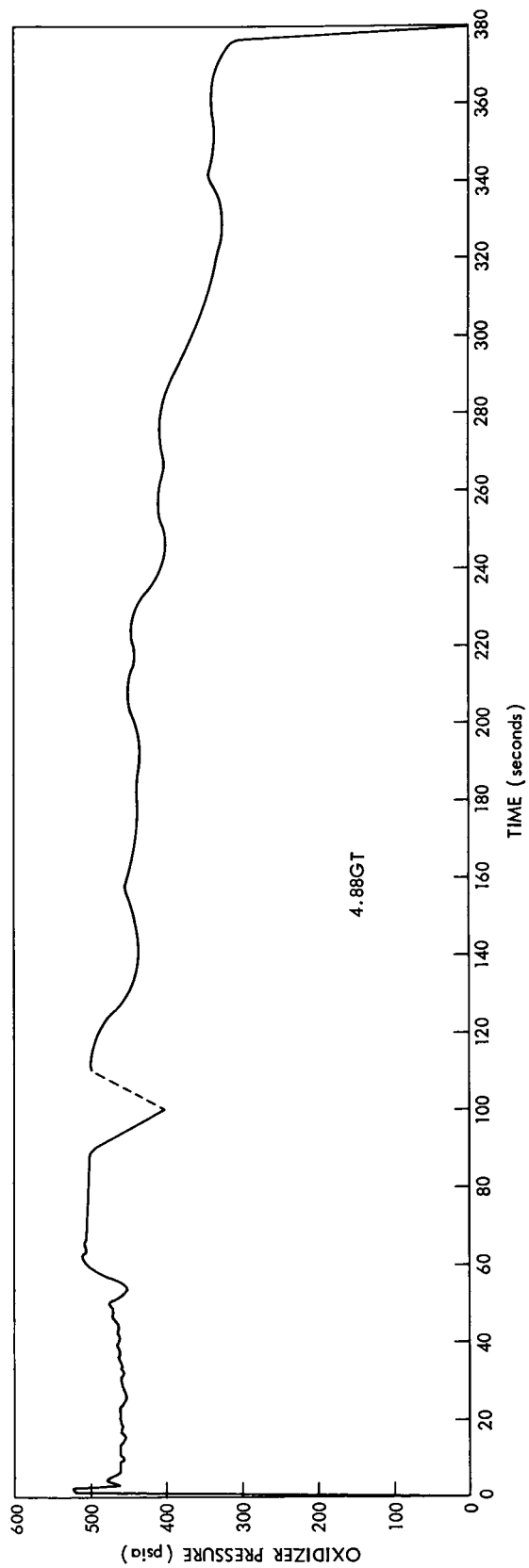
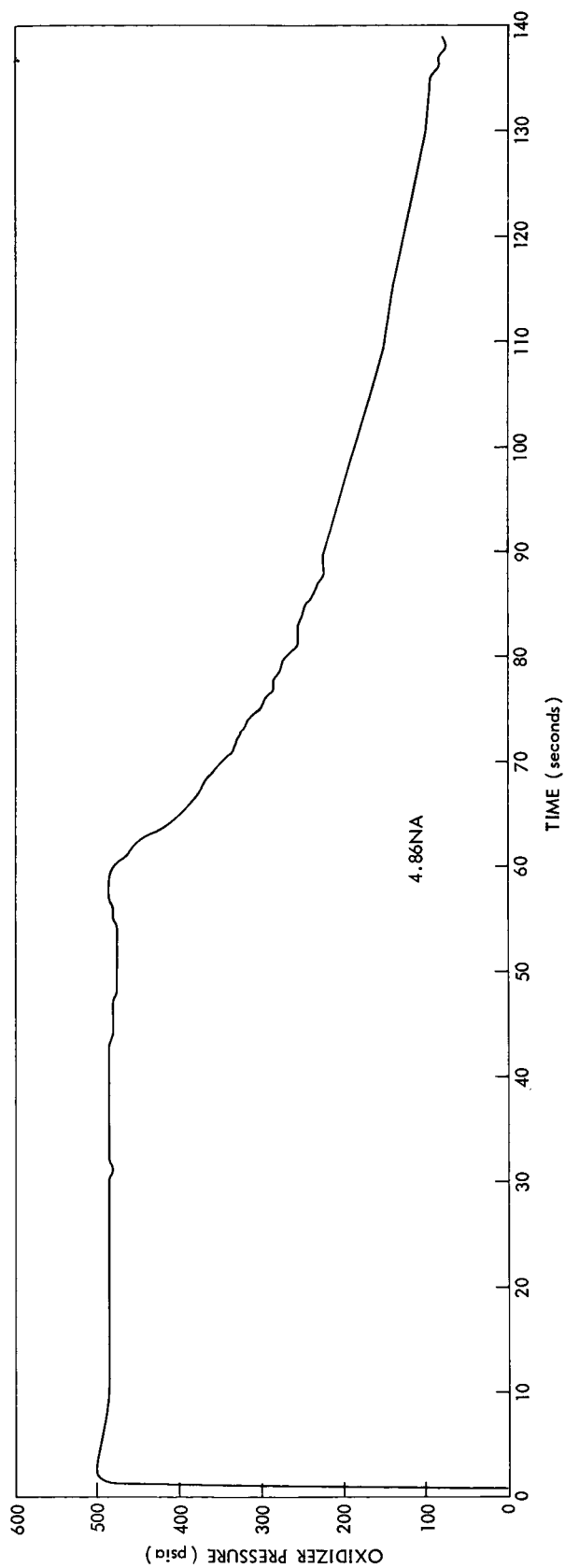


Figure A3—Oxidizer pressure vs. time; comparison of flights 4.86 NA and 4.88 GT.

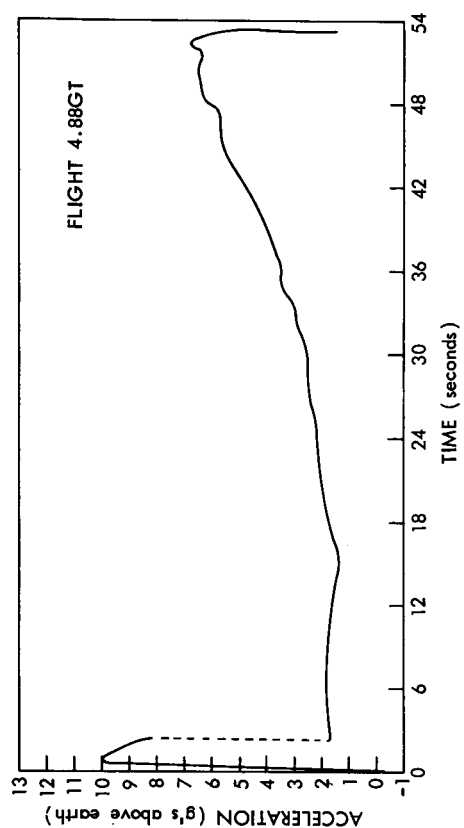
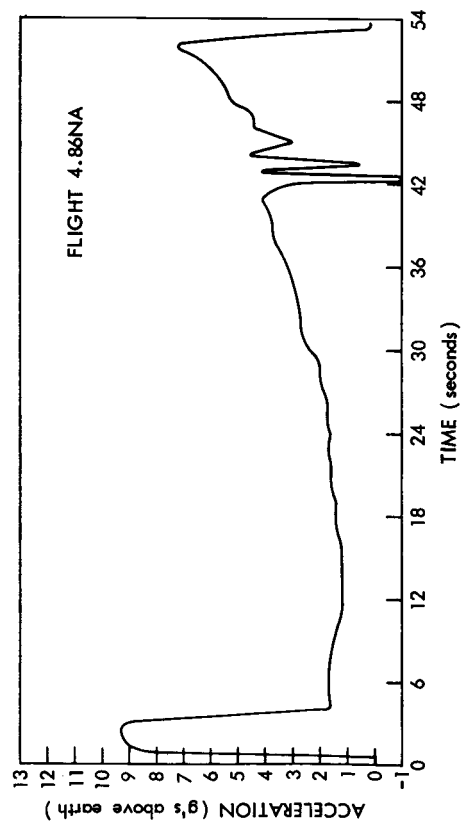
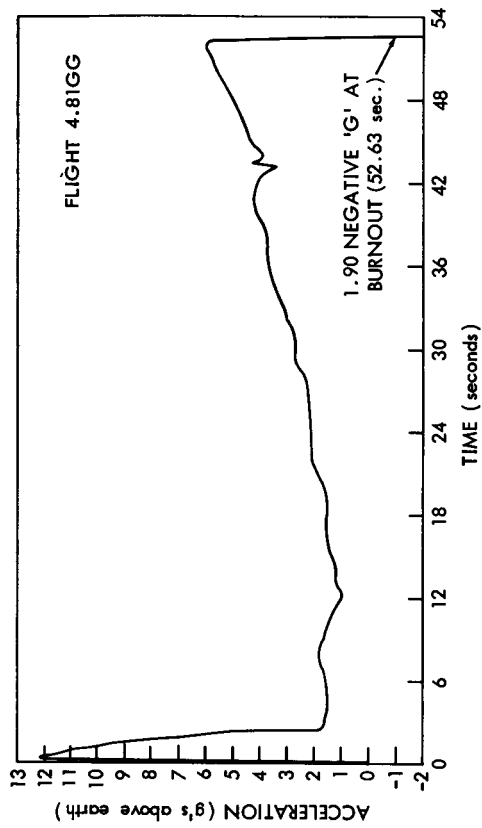
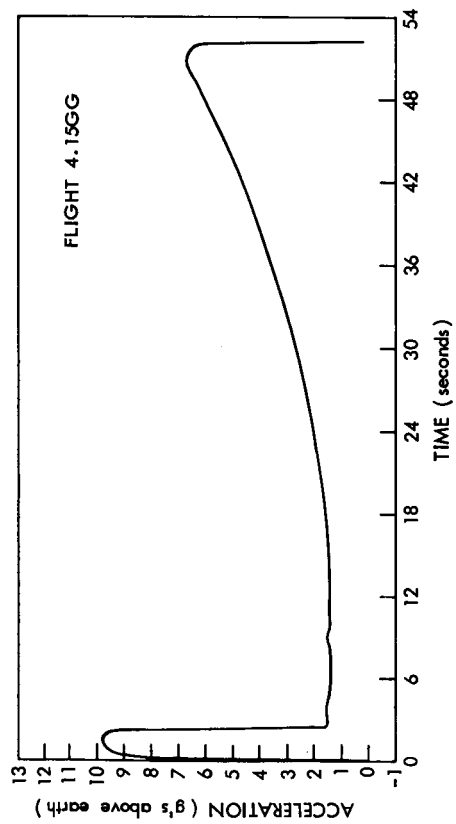


Figure A4—Acceleration vs. time; comparison of flights 4.15 GG, 4.81 GG, 4.86 NA, and 4.88 GT.

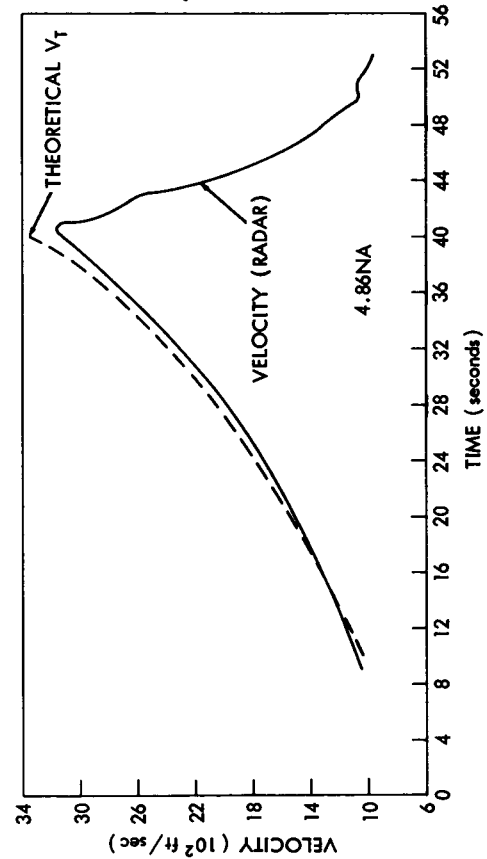
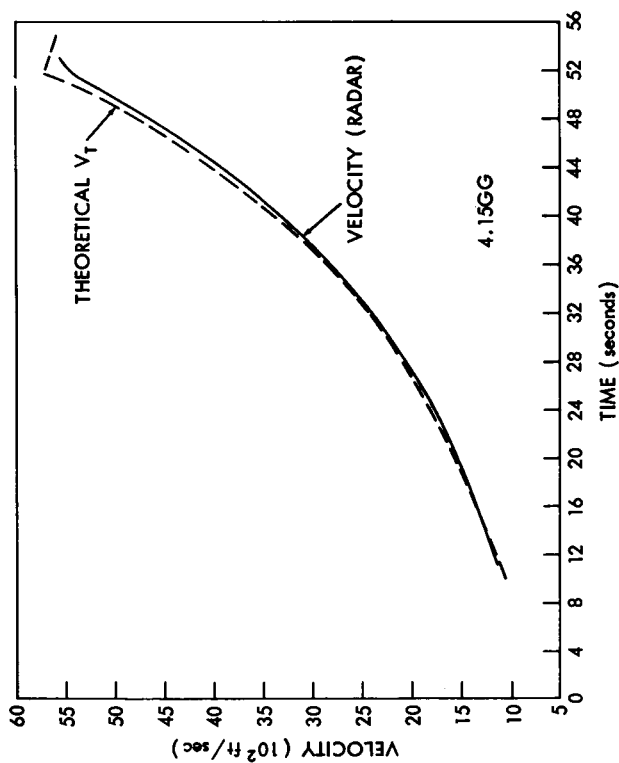
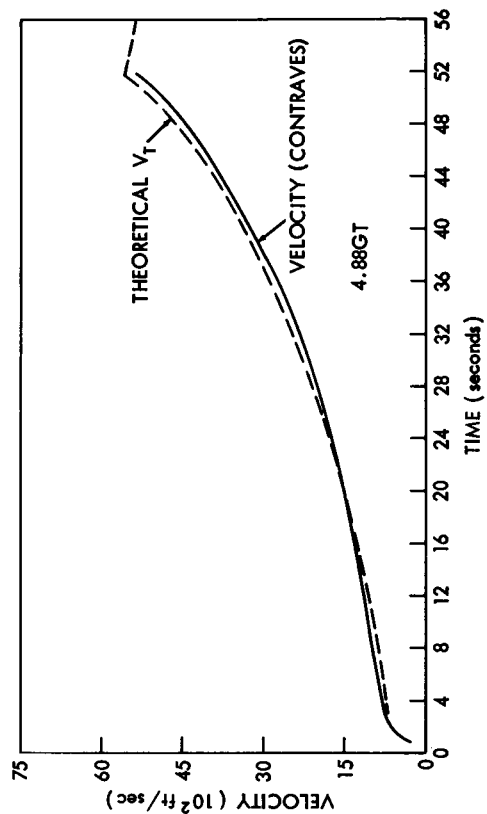
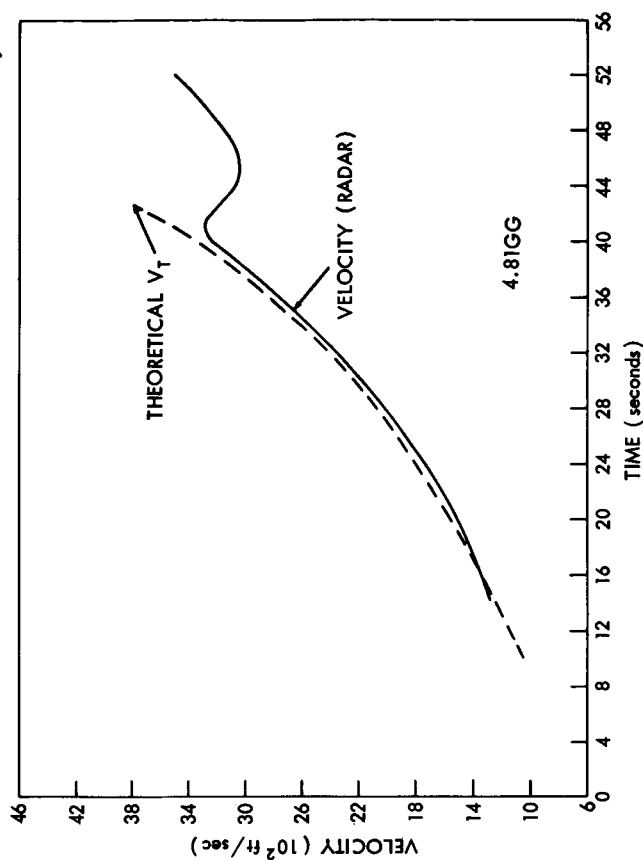


Figure A5—Vertical velocity and theoretical total velocity vs. time; comparison of flights 4.15 GG, 4.81 GG, 4.86 NA, and 4.88 GT.

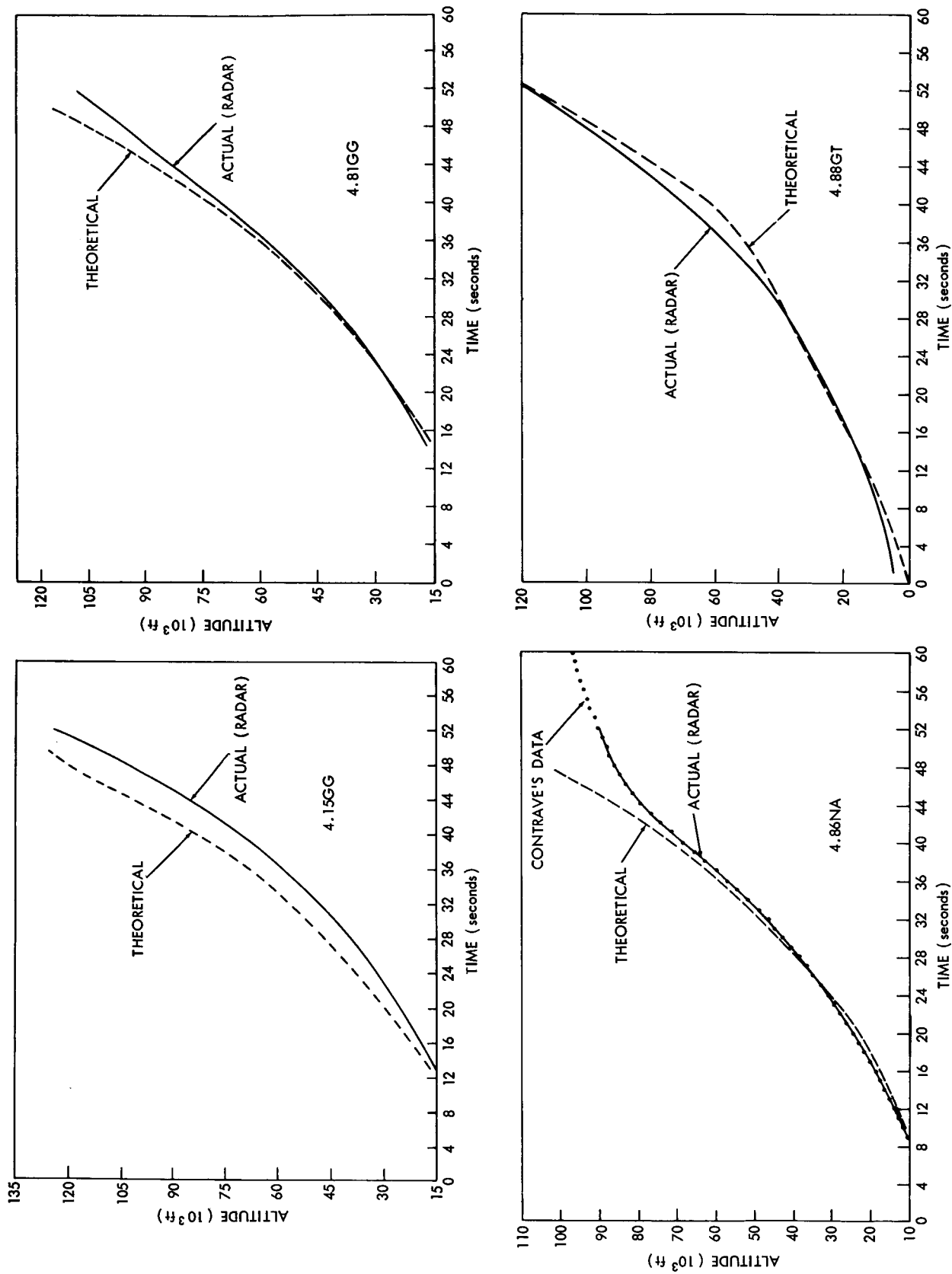


Figure A6—Altitude vs. time; comparison of flights 4.15 GG, 4.81 GG, 4.86 NA, and 4.88 GT.

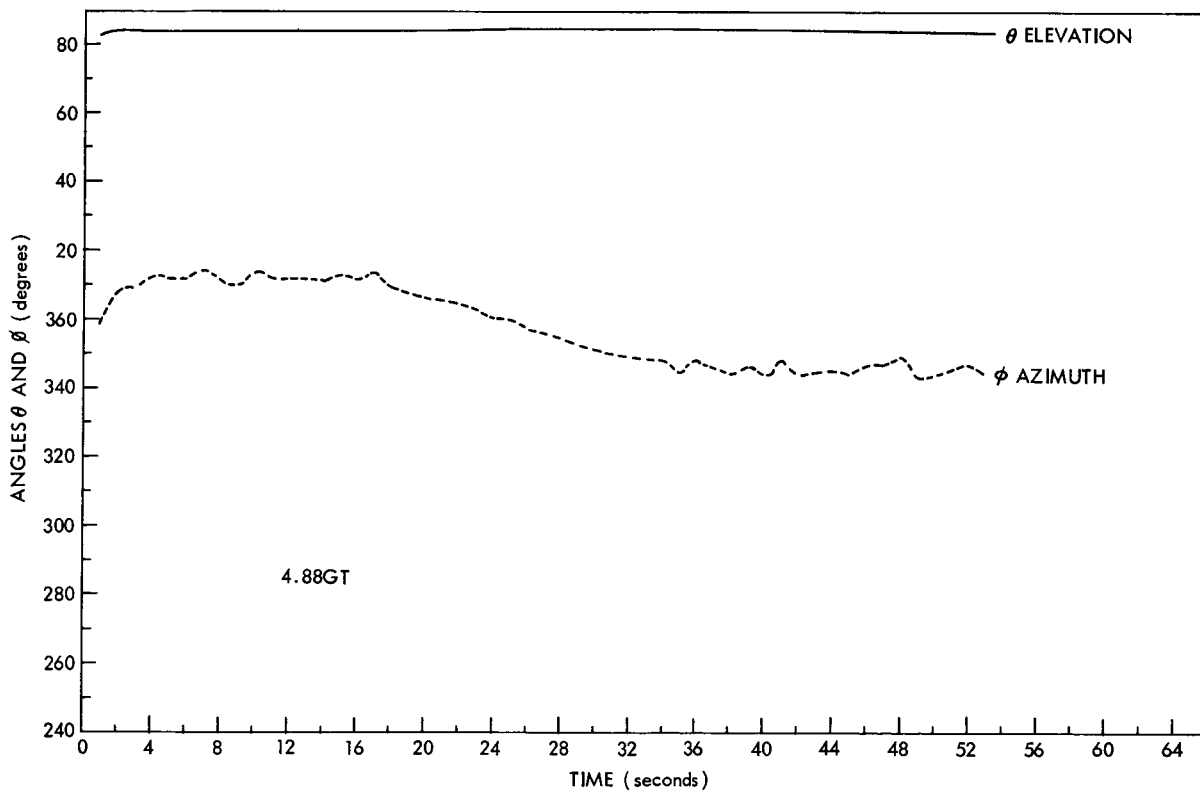
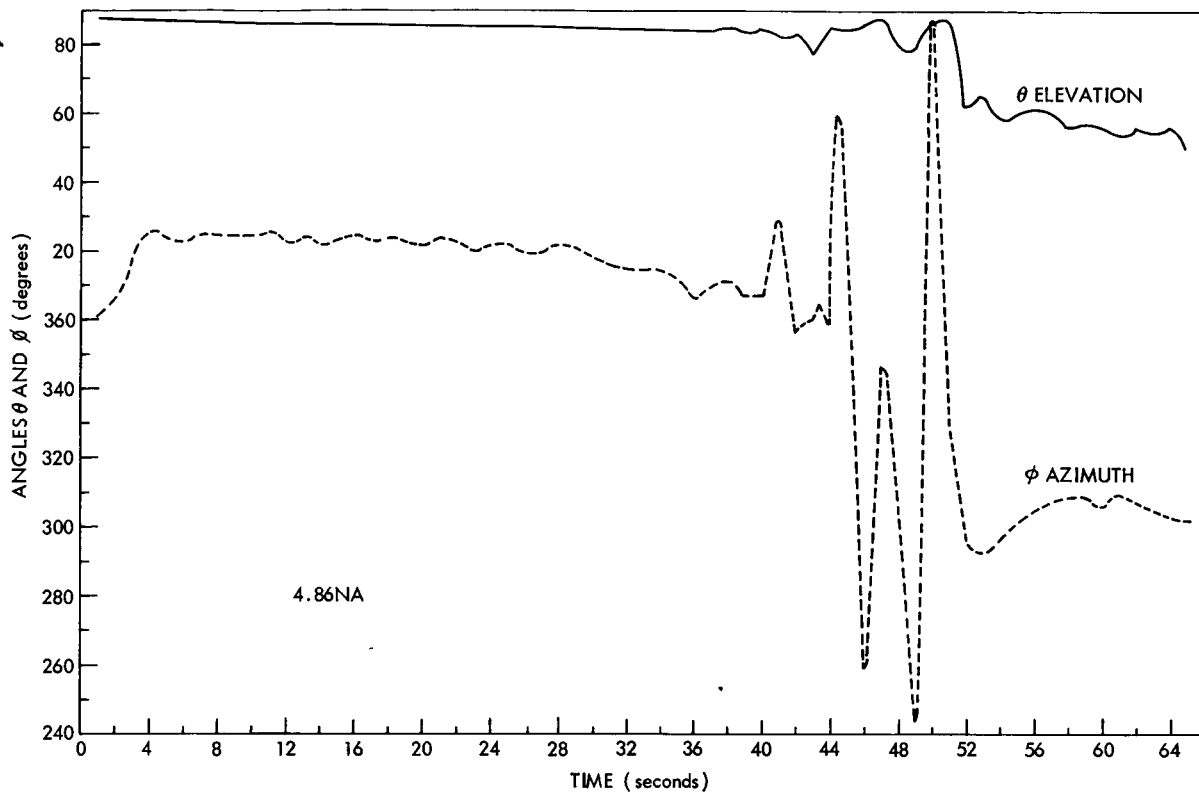


Figure A7—Velocity vector, elevation angle, and azimuth angle vs. time;
comparison of flights 4.86 NA and 4.88 GT.

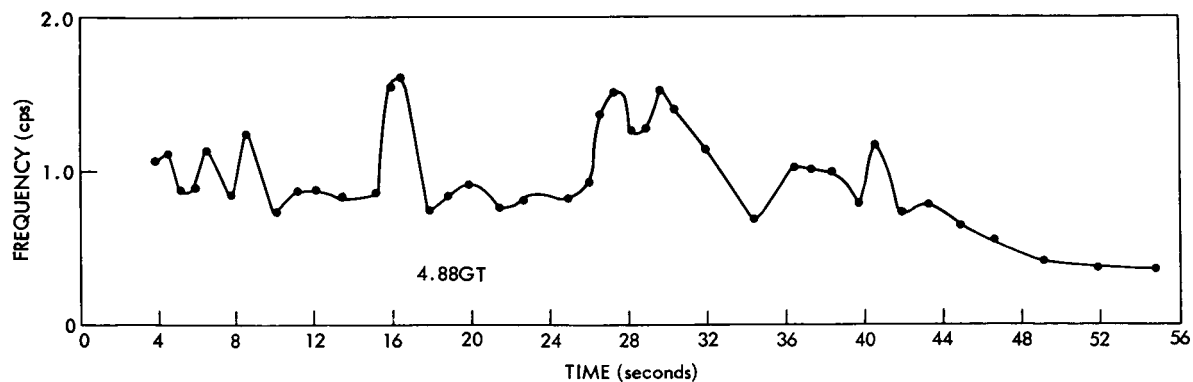
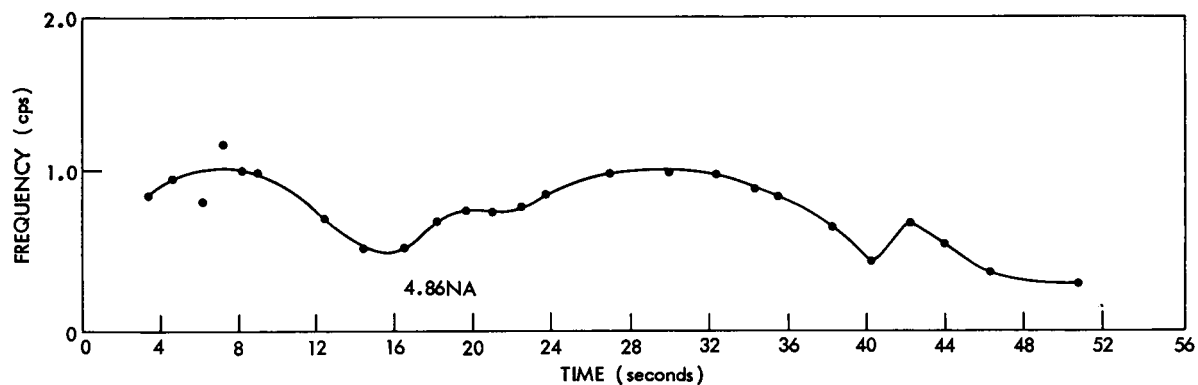
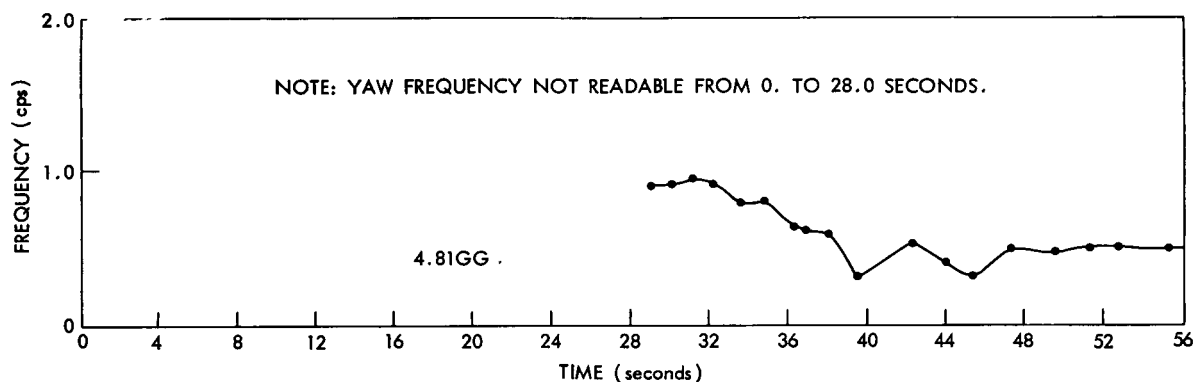
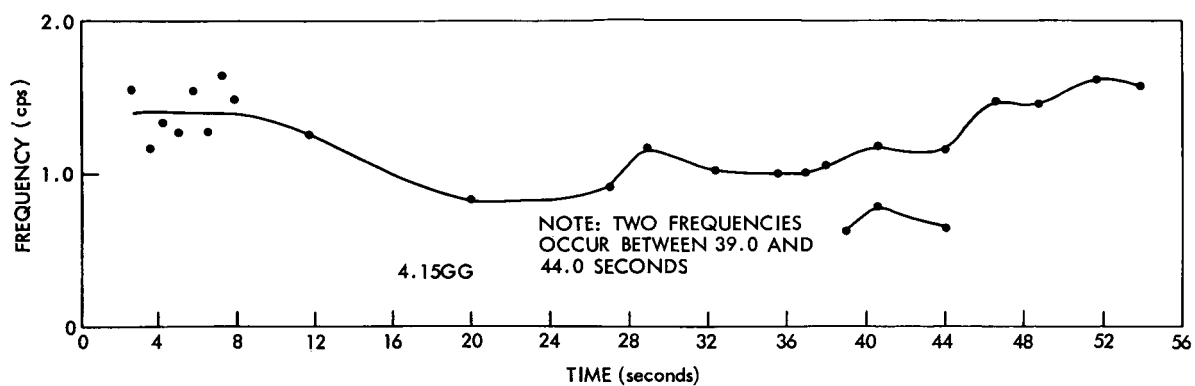


Figure A8—Yaw frequency vs. time; comparison of flights 4.15 GG, 4.81 GG, 4.86 NA, and 4.88 GT.

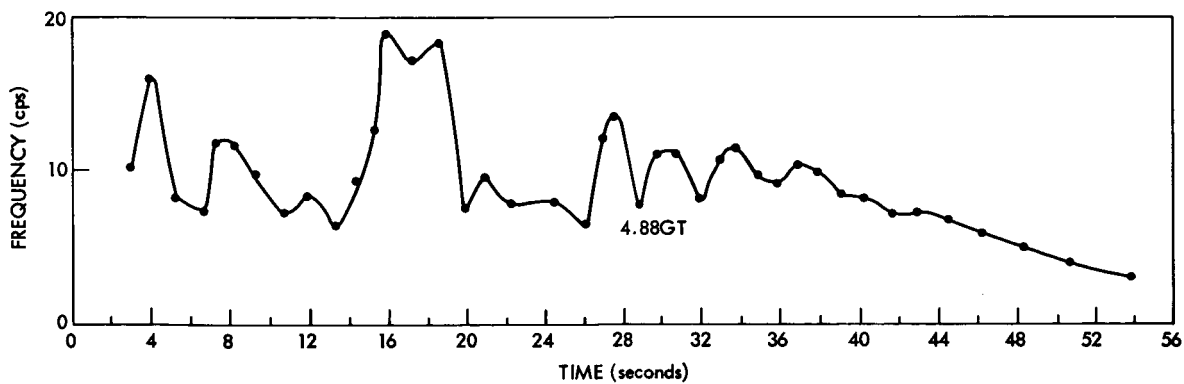
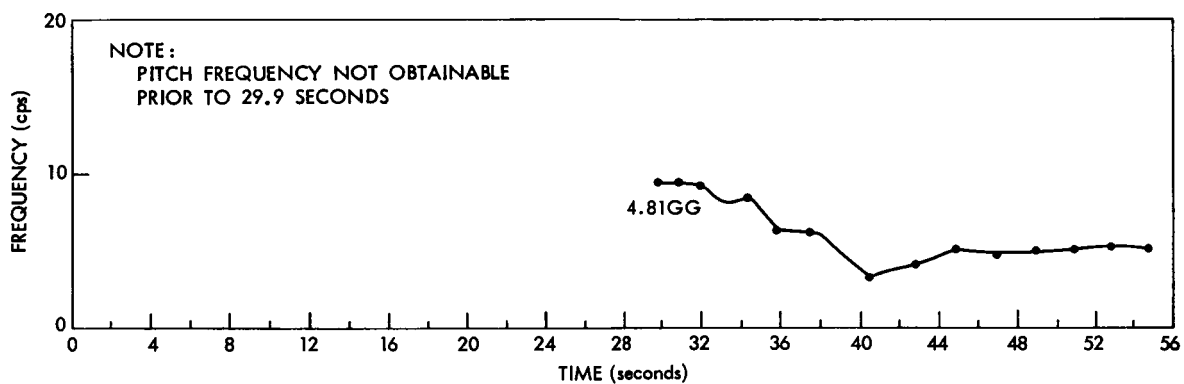
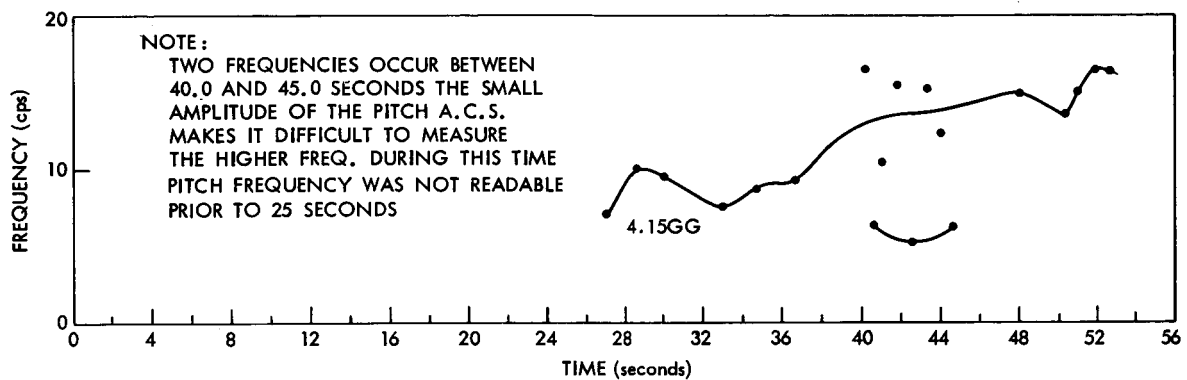


Figure A9—Pitch frequency vs. time; comparison of flights 4.15 GG, 4.81 GG, and 4.88 GT.

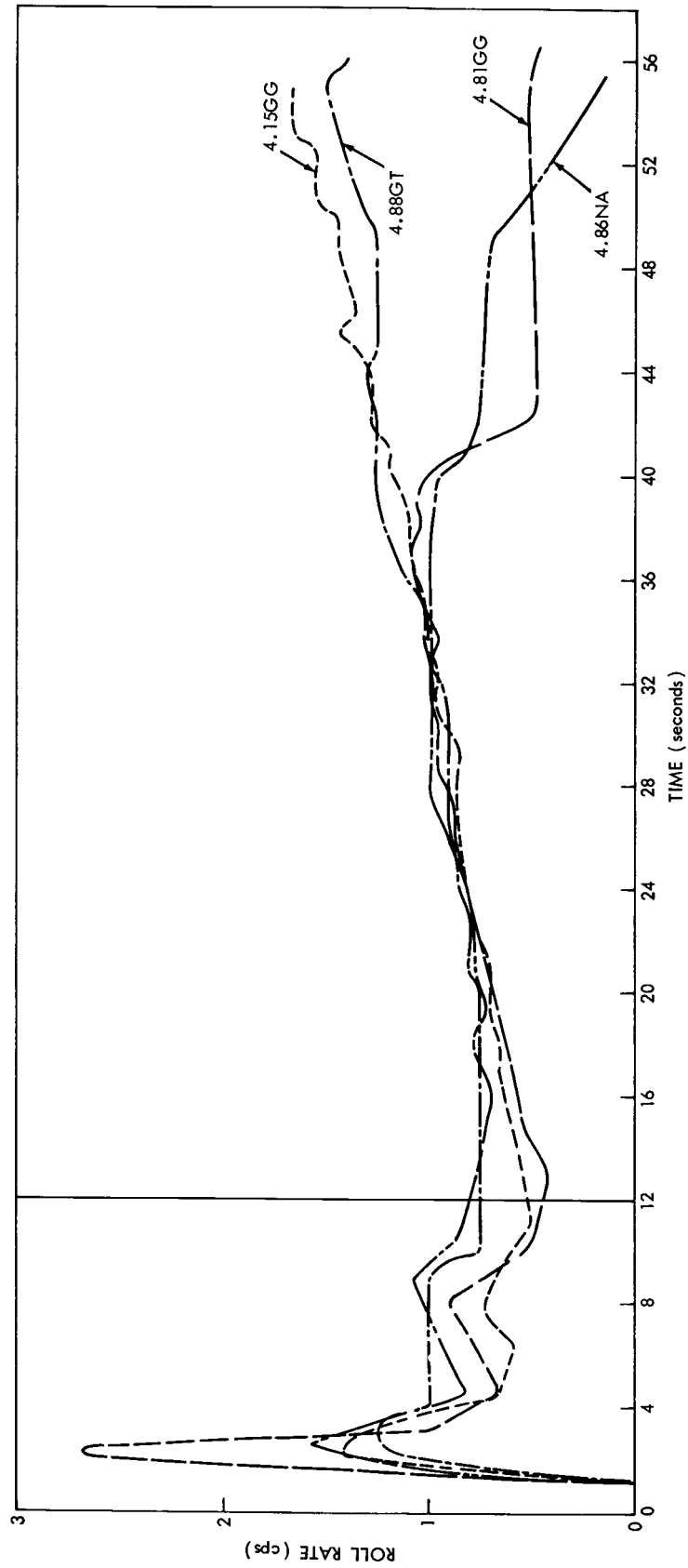


Figure A10—Roll rate vs. time; comparison of flights 4.15 GG, 4.81 GG, 4.86 NA, and 4.88 GT.

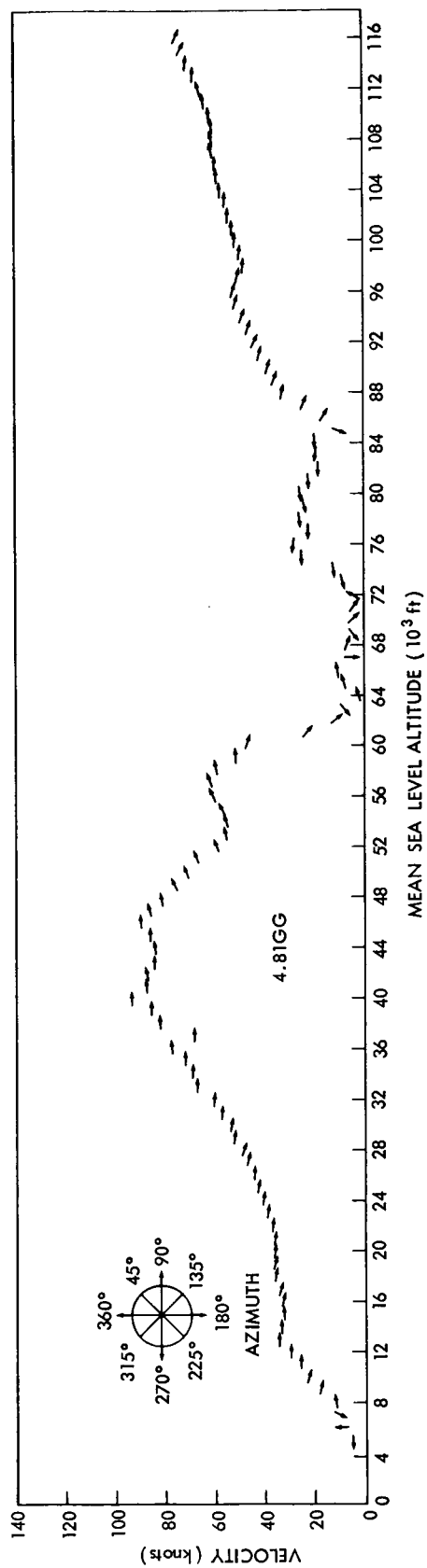
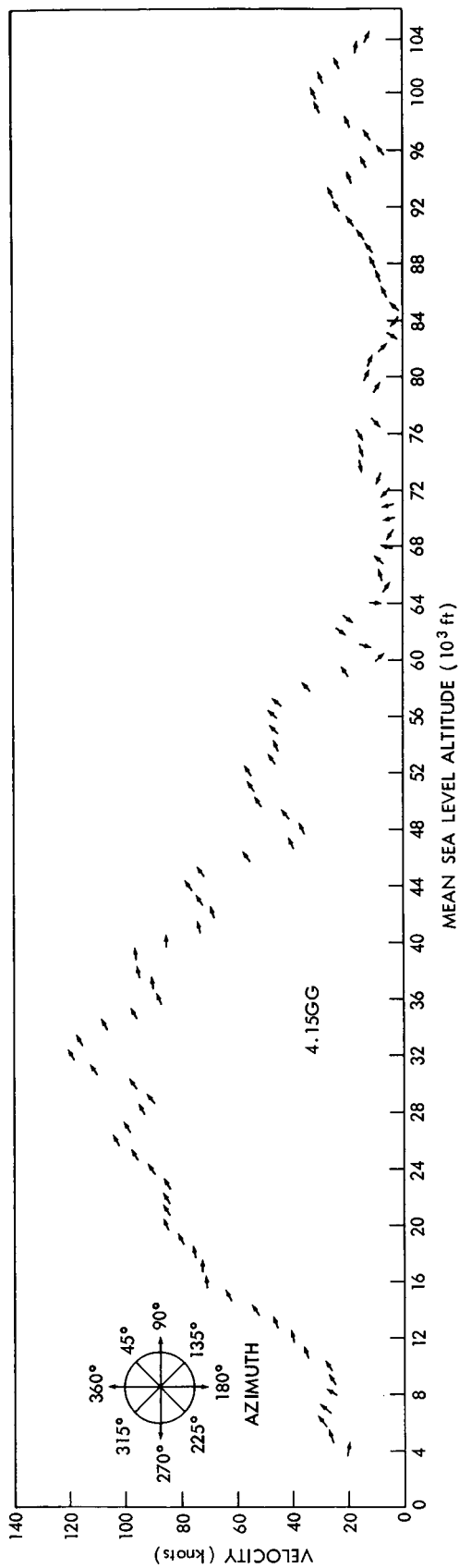


Figure A11(a)—Wind velocity and azimuth angle vs. altitude, comparison of flights 4.15 GG and 4.81 GG.

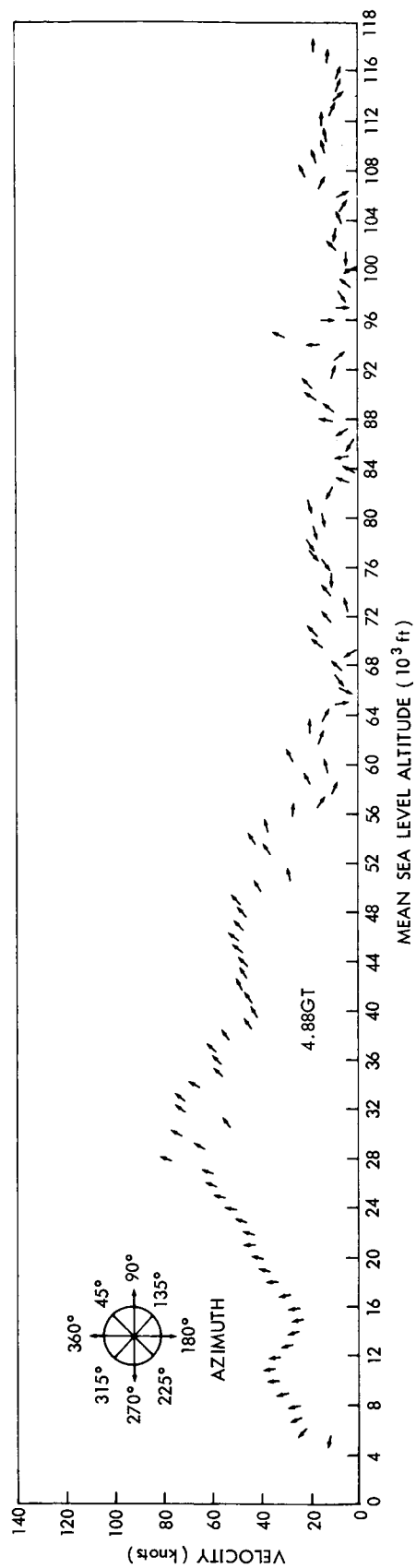
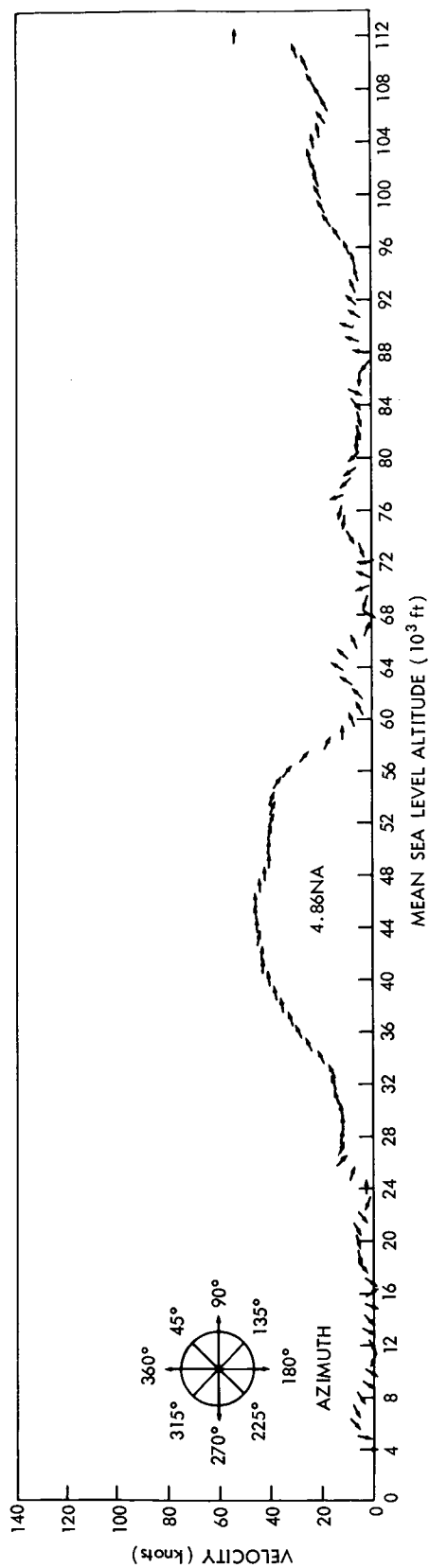


Figure A11(b)—Wind velocity and azimuth angle vs. altitude, comparison of flights 4.86 NA and 4.88 GT.

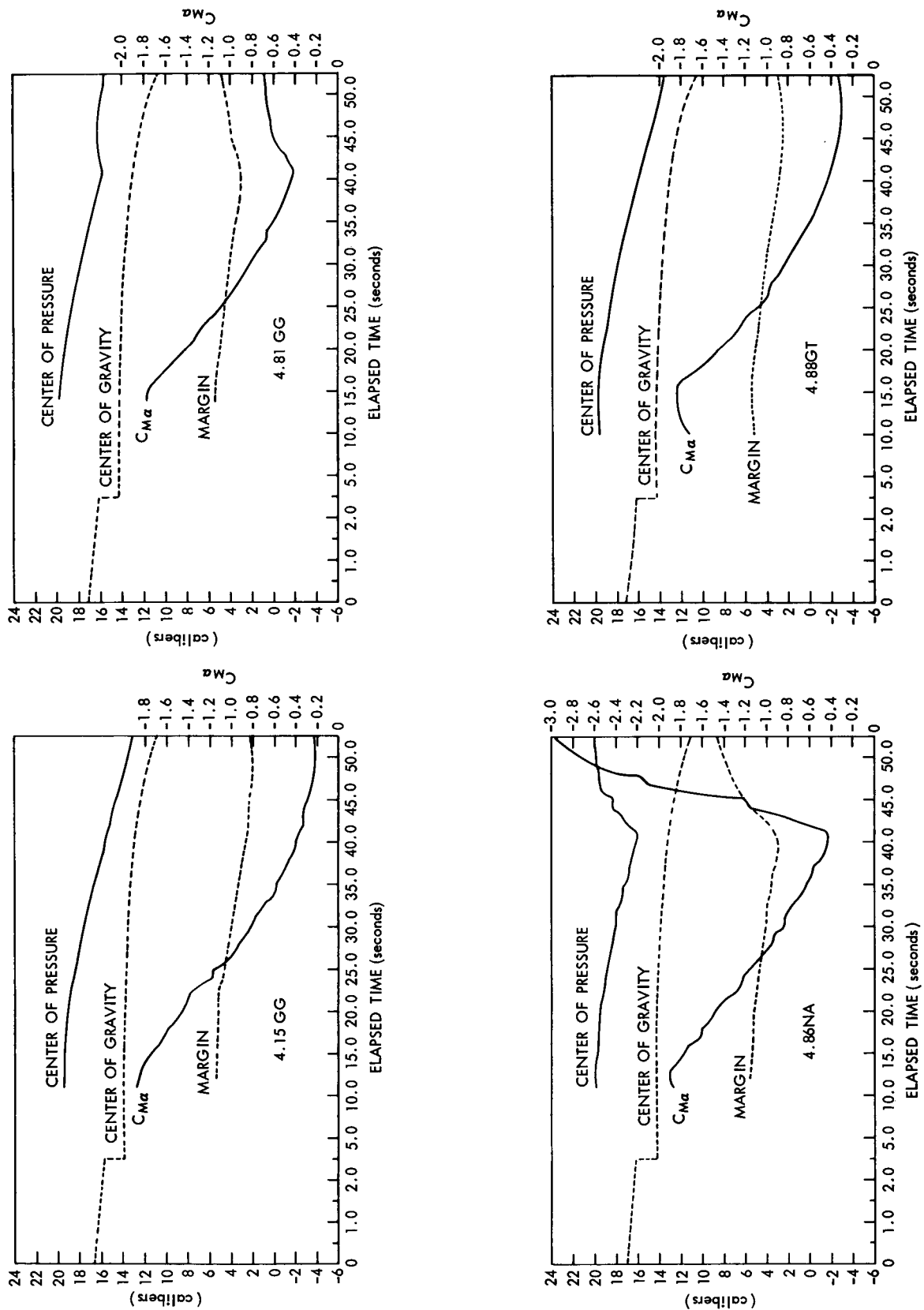


Figure A12—Center of gravity, static margin, center of pressure, and restoring moment vs. time; comparison of flights 4.15 GG, 4.81 GG, 4.86 NA, and 4.88 GT.

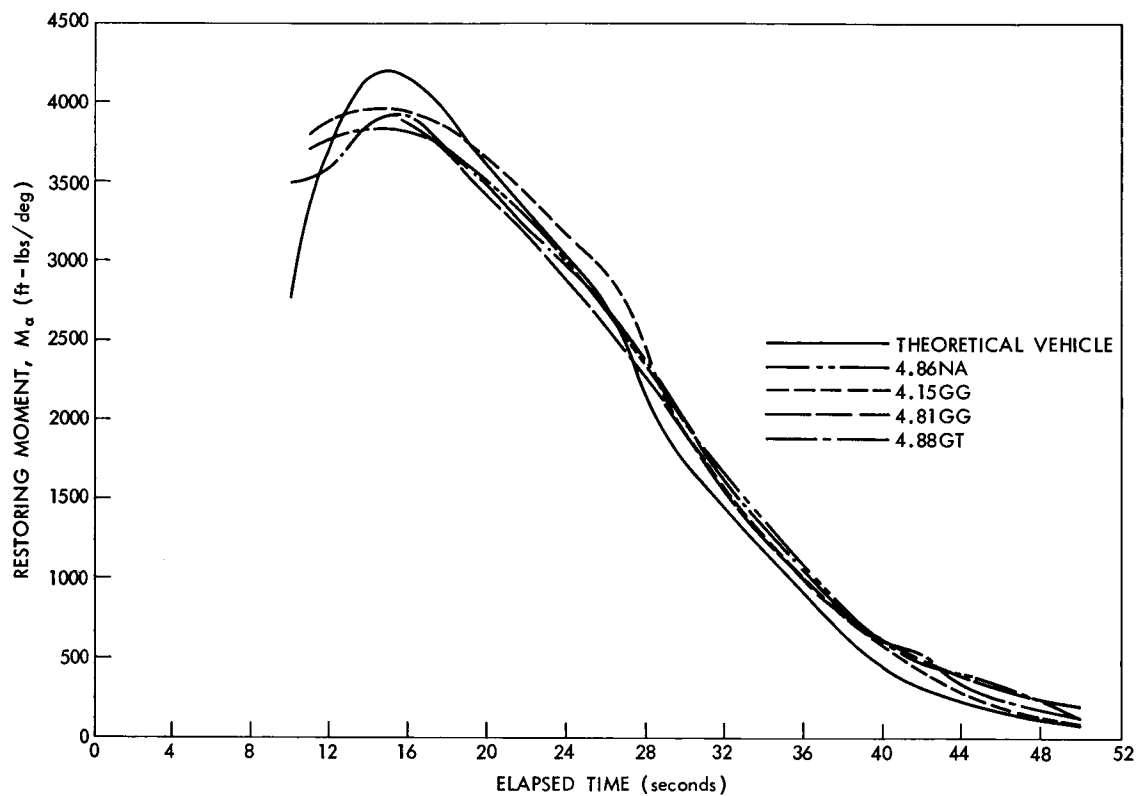


Figure A13—Restoring moment vs. time; comparison of flights 4.15 GG, 4.81 GG, 4.86 NA, and 4.88 GT, theoretical vehicle.

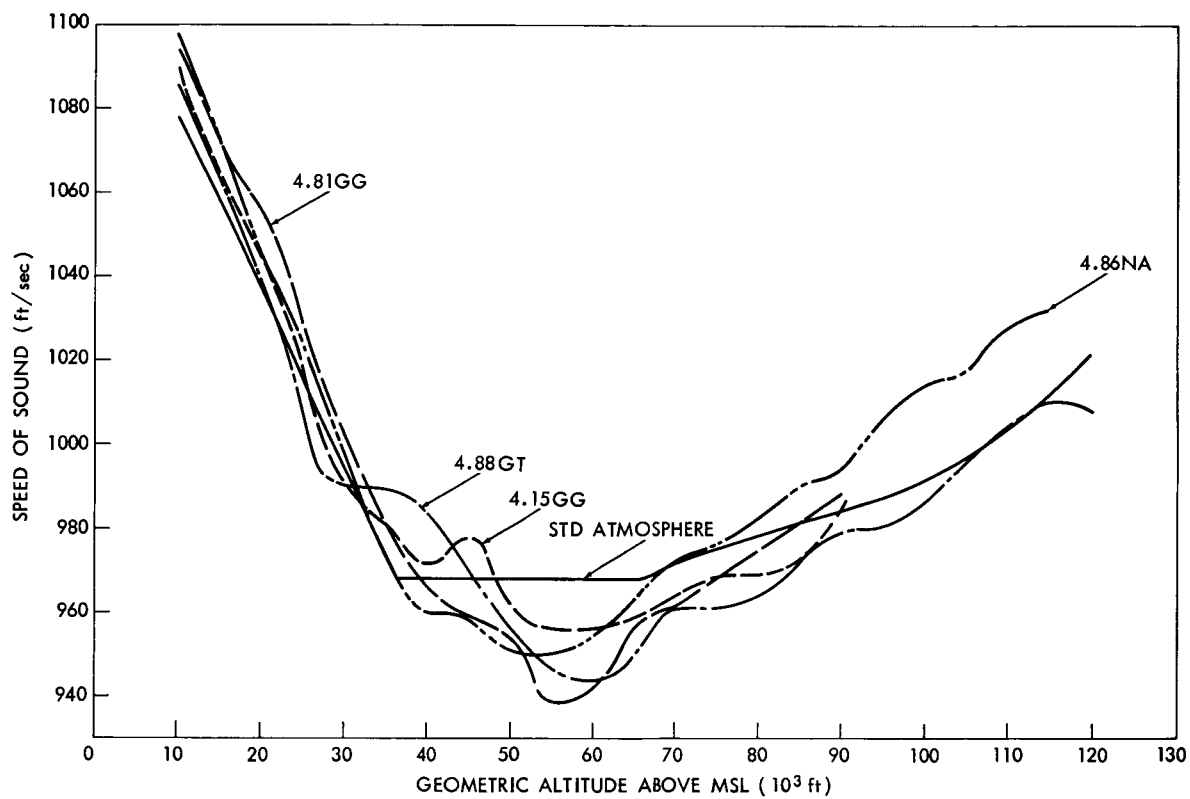


Figure A14—Speed of sound vs. altitude; comparison of flights 4.15 GG, 4.81 GG, 4.86 NA, and 4.88 GT and standard atmosphere (Reference 6).

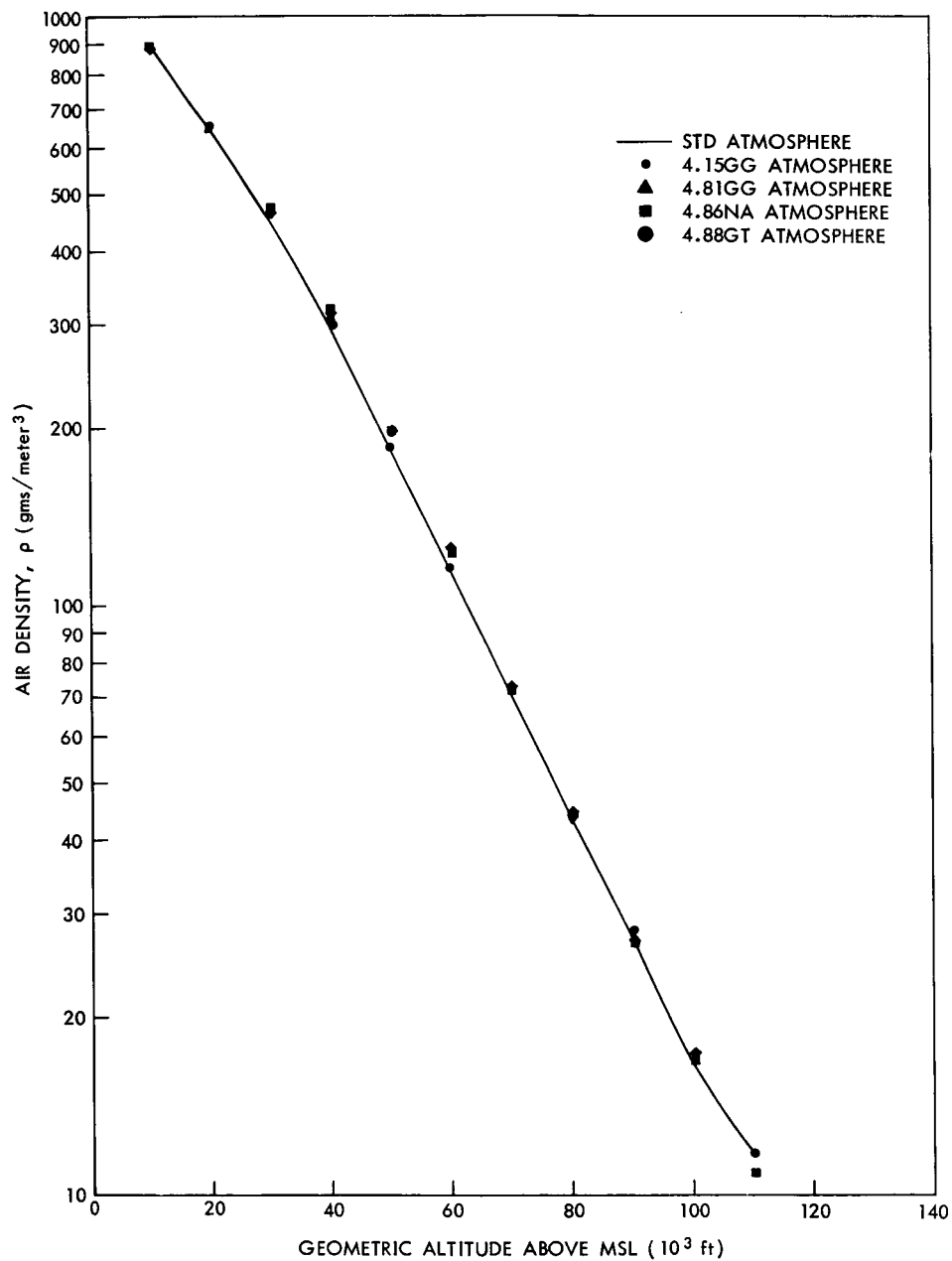


Figure A15—Atmospheric density vs. altitude; comparison of flights 4.15 GG, 4.81 GG, 4.86 NA, and 4.88 GT.

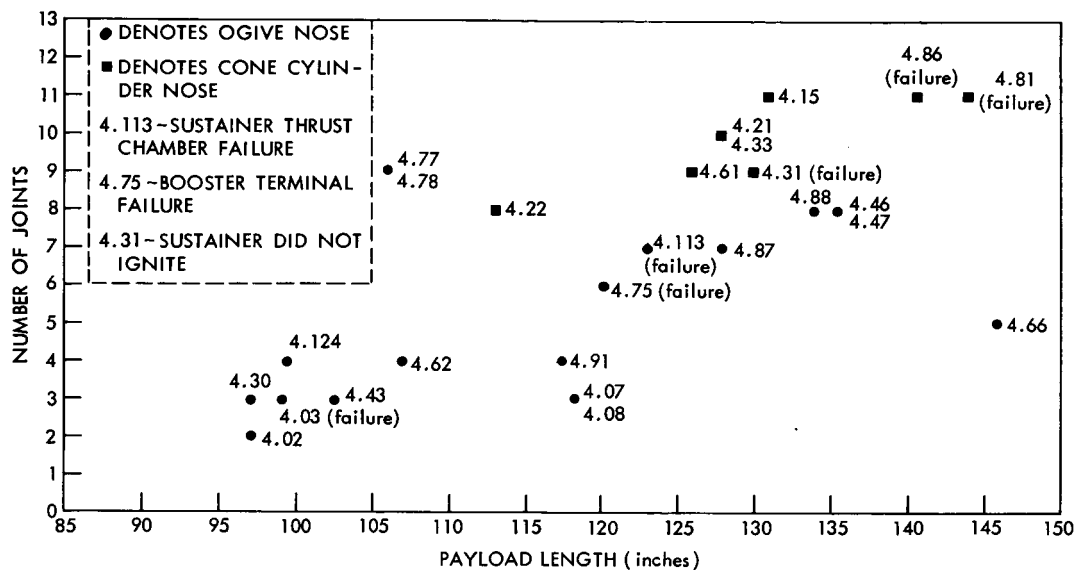


Figure A16—Number of joints in Aerobee 150 vs. payload lengths.

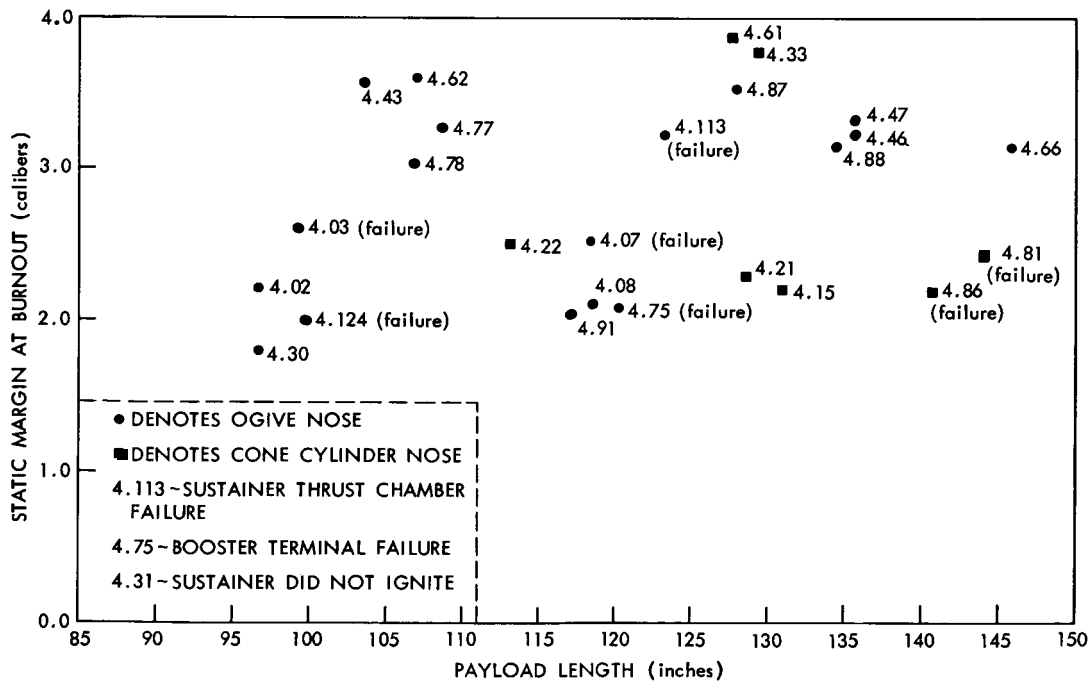


Figure A17 – Aerobee 150 static margin vs. payload length.

Appendix B

Flight Data Analysis*

Dynamic Analysis

This Appendix is included to verify the plausibility of deductions that the failures of Flights 4.81 GG and 4.86 NA were caused by dynamic coupling and later lock-in between the rocket's structural bending mode and the vehicle pitch mode. The analysis is an evaluation of the structural properties (i.e., nose joint free play and stiffness) required to produce this interaction.

To obtain the simplest meaningful physical model which could produce the desired motions, the dynamic analysis was restricted to three degrees of freedom. The lateral displacement of a point on the body longitudinal axis is represented as a superposition of rigid body translation, rigid body pitch rotation, and deflection of the nose by rotation about a point x_0 at the base of the nose. The lateral displacement is then written as:

$$z(x, t) = a_0(t) + a_1(t)x + a_2(t)(x - x_0) \ell(x - x_0),^{**} \quad (1)$$

where $\ell(x - x_0)$ is the unit step function at $x = x_0$.

Neglecting roll, the kinetic energy is given by

$$2T = m\dot{a}_0^2 + I\dot{a}_1^2 + 2r\dot{a}_0\dot{a}_2 + 2J\dot{a}_1\dot{a}_2 + I_0\dot{a}_2^2. \quad (2)$$

The Lagrangian equation of motion is then

$$\frac{d}{dt} \frac{\partial T}{\partial \dot{a}_n} - \frac{\partial T}{\partial a_n} = Q_n, \quad \text{for } n = 0, 1, 2, \quad (3)$$

where the generalized forces Q_n are given by

$$Q_0 = L_a a_1 + L_{n_a} a_2 - \frac{1}{V} (L_a \dot{a}_0 + M_a \dot{a}_1 + B_a \dot{a}_2), \quad (4)$$

$$Q_1 = M_a a_1 + L_{n_a} x_n a_2 - \frac{1}{V} (M_a \dot{a}_0 + M_q \dot{a}_1 + B_q \dot{a}_2), \quad (5)$$

*Based on an analysis performed by A. W. Earnest of the Space General Corporation.

**A list of symbols used in this analysis is provided at the end of this appendix.

and

$$Q_2 = B_a a_1 + B_a a_2 - \frac{1}{V} (B_a \dot{a}_0 + B_q \dot{a}_1 + B_\delta \dot{a}_2) - k a_2 \quad (6)$$

These are derived by using

$$\alpha(x) = \frac{\partial z(x, t)}{\partial x} - \frac{1}{V} \dot{z}(x, t) = a_1 + a_2 1(x - x_0) - \frac{1}{V} (\dot{a}_0 + \dot{a}_1 x + \dot{a}_2 (x - x_0)) \ell(x - x_0) \quad (7)$$

and assuming the lift distribution $\ell(x)$ to be adequately represented by two concentrated loads:

$$\ell(x) = L_{n_a} \alpha(x_n) \delta(x - x_n) + L_{t_a} \alpha(x_t) \delta(x - x_t) \quad (8)$$

where $\delta(x)$ is the Dirac delta function. Inserting Equations 4, 5, and 6 into Equation 3, the equations of motion are found, in matrix form, to be

$$\begin{bmatrix} m & 0 & r \\ 0 & I & J \\ r & J & I_0 \end{bmatrix} \Omega^2 + \begin{bmatrix} L_a & M_a & B_a \\ M_a & M_q & B_q \\ B_a & B_q & B_\delta \end{bmatrix} \frac{\Omega}{V} + \begin{bmatrix} 0 & -L_a & -L_{n_a} \\ 0 & -M_a & -L_{n_a} x_n \\ 0 & -B_a & -B_a + k \end{bmatrix} [A] = 0 \quad (9)$$

where we have set

$$a_n = A_n e^{i\Omega t} \quad \text{for } n = 0, 1, \text{ and } 2, \quad (10)$$

with A_n independent of time, and

$$[A] = \begin{bmatrix} A_0 \\ A_1 \\ A_2 \end{bmatrix} \quad (11)$$

The required input parameters are

$$\begin{aligned} B_a &= 22,900 \text{ lb-ft}, \\ B_q &= 237,000 \text{ lb-ft}^2, \\ B_\delta &= 117,400 \text{ lb-ft}^2, \\ I &= 1021 \text{ slug-ft}^2, \\ I_0 &= 139.8 \text{ slug-ft}^2, \end{aligned}$$

$$\begin{aligned}
J &= 244.9 \text{ slug-ft}^2, \\
L_a &= 15,260 \text{ lb}, \\
L_{n_a} &= 4460 \text{ lb}, \\
m &= 24.87 \text{ slugs}, \\
M_a &= -61,300 \text{ lb-ft}, \\
M_q &= 5,851,000 \text{ lb-ft}^2, \\
r &= 20.15 \text{ slug-ft}, \\
v &= 3220 \text{ fps},
\end{aligned}$$

and

$$x_n = 10.36 \text{ ft.}$$

The spring constant k is left as a free parameter. The flight conditions considered are those at $t = 37$ seconds (around the normal roll coupling point). Using these inputs, Equation 9 becomes

$$\begin{bmatrix} 24.87 & 0 & 20.15 \\ 0 & 1021 & 244.9 \\ 20.15 & 244.9 & 139.8 \end{bmatrix} \Omega^2 + \begin{bmatrix} 4.74 & -19.02 & 7.11 \\ -19.02 & 1820 & 73.5 \\ 7.11 & 73.5 & 36.5 \end{bmatrix} \Omega - \begin{bmatrix} 0 & 15,260 & 4460 \\ 0 & -61,300 & 46,200 \\ 0 & 22,900 & 22,900 - k \end{bmatrix} [A] = 0. \quad (12)$$

Setting the determinant of the matrix equal to zero and expanding, we obtain

$$1 + k \frac{F(\Omega)}{G(\Omega)} = 0, \quad (13)$$

where

$$F(\Omega) = 0.0254 \Omega^3 + 0.05005 \Omega^2 + 1.532 \Omega, \quad (14)$$

and

$$G(\Omega) = 1.645 \Omega^5 + 5.53 \Omega^4 + 46.5 \Omega^3 - 841 \Omega^2 - 41,650 \Omega + 25,100. \quad (15)$$

Equation 13 is amenable to root-locus techniques. The zeros, found by setting $F(\Omega) = 0$, are at

$$\Omega = 0, -0.985 \pm 7.47 i.$$

The poles, found by setting $G(\Omega) = 0$, are at

$$\Omega = 0.596, 11.96, -12.2, -1.853 \pm 13.10 i.$$

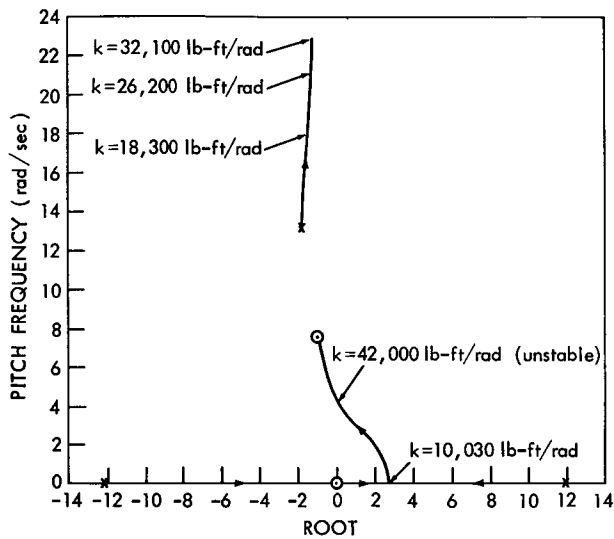


Figure B1—Pitch-mode root locus plot.

Figure B1 is a sketch of the resulting root locus plot. In this figure $k = 0$ at the poles and $k = \infty$ at the zeroes.

As may be seen in Figure B1, the pitch mode becomes unstable at $k = 42,000$ lb-ft/rad. The pitch frequency at this point is approximately $-i\Omega = 4.2$ rad/sec. We wish to find the modal coefficient ratios for this condition. Using the first two algebraic equations represented by Equation 12, we may solve for a_0/a_1 and a_2/a_1 to obtain

$$a_0/a_1 = 47.0 \angle 181.072^\circ ,$$

and

$$a_2/a_1 = 1.140 \angle -14.87^\circ .$$

Substituting these results into the third equation represented by Equation 12, we may solve for k as a check on the solution. This yields

$$k = 34,200 \angle 4.81^\circ .$$

It will be noted that k is not quite a pure real quantity and that this magnitude does not agree well with the 42,000 figure obtained from Figure B1. This may be attributed to expanding 3 by 3 determinants and factoring fifth-order polynomials by use of a 10-inch slide rule and to the accuracy of the graphical solutions of Figure B1. If Ω is increased to 4.3 i, we obtain

$$a_0/a_1 = 45.0 \angle 178.562^\circ .$$

$$a_2/a_1 = 1.162 \angle -15.3^\circ ,$$

and

$$k = 37,600 \angle 17.1^\circ ,$$

so the magnitude of k is brought into somewhat better agreement with Figure B1, but the phase angle becomes worse. Extrapolating these two results to zero phase angle for k yields

$$a_0/a_1 = 44.8 \angle 182^\circ ,$$

$$a_2/a_1 = 1.132 \angle -14.7^\circ ,$$

and

$$k = 31,800 .$$

We may, with certainty, conclude only that

$$45.0 \angle 178.6^\circ \leq a_0/a_1 \leq 47.8 \angle 182^\circ ,$$

$$1.132 \angle -14.7^\circ \leq a_2/a_1 \leq 1.162 \angle -15.3^\circ ,$$

and

$$31,800 \leq k \leq 42,000 .$$

The variations in a_0/a_1 and a_2/a_1 are not serious, but the spread in k is rather severe. Note that the upper branch of Figure B1 would have $\Omega \approx 27$ i at $k = 42,000$.

Static Aeroelastic Analysis*

In order to obtain the usual static aeroelastic solution, we use the equations of motion developed for the dynamic analysis, with the constraints

$$\dot{a}_0 = \dot{a}_1 = \dot{a}_2 = 0$$

and

$$\ddot{a}_2/\ddot{a}_1 = a_2/a_1 .$$

The equations may then be solved for a_2/a_1 to yield

$$a_2/a_1 = \frac{25,270}{k - 8230}$$

for the flight conditions considered. Using this result, the variations in static margin may be determined. These are plotted in Figure B2.

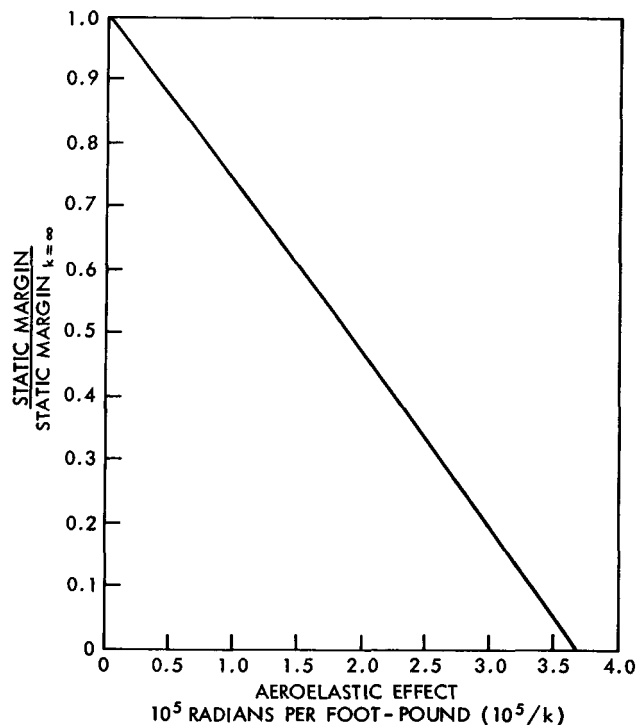


Figure B2—Static aeroelastic effect on static margin.

*The input data used for these analyses were data representative of flights 4.81 GG and 4.86 NA. This method of analysis was used to analyze the NASA flight 4.67 NP configuration (the next rocket to be launched after the failures of 4.81 GG and 4.86 NA). NASA 4.67 NP was successfully flown in June of 1964 with a configuration similar to 4.81 GG and 4.86 NA, but incorporating the changes specified in the conclusions of the main report.

Note that the frequency of oscillation of the pitch branch in the curves of Figure B1 is also a good measure of static margin and agrees fairly well with Figure B2.

Conclusions

The following conclusions are drawn from the analyses presented herein:

1. The basic physical mechanism of dynamic coupling of pitch and structural bending modes seems to be correct and the frequency/stability relationship appears to correspond to flight data from 4.81 GG.

2. The bending/pitch amplitude ratio at the structurally stable point seems unreasonable in that free joint play on the order of $\pm 3^\circ$ would be required to explain Flight 4.81 GG.

3. The most probable cause of disagreement between the analysis and the flight data, with respect to amplitude (assuming the amplitude of $\pm 3^\circ$ is incorrect), is the omission of roll effects from these analyses.

The basic physical mechanism for the dynamic coupling of pitch and structural bending modes is correct and does indeed produce such frequency/stability relationships as those observed in flight data for the failed flights.

Symbols

<u>Symbol</u>	<u>Definition</u>	<u>Unit</u>
A	Nose deflection angle divided by free play deflection limit	--
a_n	Modal coefficient of nth mode	ft ($n=0$)
B_α	$L_{n_\alpha} (x_n - x_0)$	lb-ft
B_δ	$L_{n_\alpha} (x_n - x_0)^2$	lb-ft ²
B_q	$L_{n_\alpha} x_n (x_n - x_0)$	lb-ft ²
I	Vehicle transverse moment of inertia	slug-ft ²
I_0	Moment of inertia of portion of vehicle forward of x_0 , taken about $x = x_0$	slug-ft ²
J	$I_0 + m_0 x_0 (\bar{x}_0 - x_0)$	
k	Nose joint spring constant	lb-ft/rad
L_α	Total lift per unit rigid angle of attack	lb
L_{n_α}	Nose lift per unit angle of attack	lb
L_{t_α}	Tail lift per unit angle of attack	lb
ℓ	Running airload	lb/ft
M_α	Pitching moment per unit rigid angle of attack	lb-ft

<u>Symbol</u>	<u>Definition</u>	<u>Unit</u>
M_q	$x_n^2 L_{n_a} + x_t^2 L_{t_a}$	lb-ft ²
m	Vehicle total mass	slug
m_0	Mass forward of $x = x_0$	slug
Q_n	Generalized force for the n th mode	lb ($n=0$) lb-ft ($n=1$) lb-ft ² ($n=2$)
r	$m_0(\bar{x}_0 - x_0)$	--
T	Kinetic energy	slug-ft ² /sec ²
t	Time	sec
V	Flight velocity	ft/sec
x	Coordinate along body centerline, zero at c.g., positive forward	ft
x_0	x at nose joint	ft
x_n	x at nose center of pressure	ft
x_t	x at tail center of pressure	ft
\bar{x}_0	x at c.g. of mass forward of x_0	ft
z	Lateral displacement	ft
α	Angle of attack	rad
δ	Joint free play rotation	rad
Ω	Complex frequency	rad/sec
ω	Natural bending frequency	rad/sec or cps

Appendix C

Definition of Terms

These definitions are included, since explicit word definitions have not previously been established by the technical community for Aerobee rocket applications.

Yaw (Pitch)-Roll Resonance

The time at which the rocket's aerodynamic natural pitching frequency and roll frequency are equal.

Yaw (Pitch)-Roll Coupling

The establishment of a dynamic interaction between the roll and yaw (pitch) frequencies of the rocket which occurs immediately after yaw (pitch)-roll resonance. Yaw (pitch)-roll coupling does not produce catastrophic rocket motion.

Yaw (Pitch)-Roll Lock-In

A result of the yaw (pitch)-roll coupling phenomenon which exists when the rocket is coupled for an extended period of time and is accompanied by larger quasi-precessional rocket yawing (pitching) motion.

Catastrophic Yaw (Pitch)

A condition producing catastrophic (excessively large) quasi-precessional rocket motion which is always preceded by yaw (pitch)-roll lock-in.

Bimodal Coupling

A dynamic interaction between the aerodynamic natural pitching frequency and one of the "complex" structural frequencies of the rocket.

Bimodal Instability

The result of the bimodal coupling which produces an increasing quasi-precessional rocket motion, detrimental to rocket performance, and is a mechanism for producing yaw (pitch)-roll coupling, yaw (pitch)-roll lock-in, and potentially catastrophic yaw (pitch).